Brain Struct Funct (2016) 221:3803–3823
DOI 10.1007/s00429-016-1191-3

ORIGINAL ARTICLE

# Comparative anatomical distribution of neuronal calcium-binding protein (NECAB) 1 and -2 in rodent and human spinal cord

**Ming-Dong Zhang[1,2] · Swapnali Barde[1] · Edit Szodorai[3,7] · Anna Josephson[1] · Nicholas Mitsios[4] · Masahiko Watanabe[5] · Johannes Attems[6] · Gert Lubec[7] · Gábor G. Kovács[8] · Mathias Uhlén[4,9] · Jan Mulder[4] · Tibor Harkany[2,3] · Tomas Hökfelt[1]**

Received: 16 August 2015 / Accepted: 18 January 2016 / Published online: 2 February 2016


**Abstract** Neuronal calcium-binding protein 1 and -2 (NECAB1/2) localize to multiple excitatory neuron populations in the mouse spinal cord. Here, we analyzed rat and human spinal cord, combining in situ hybridization and immunohistochemistry, complementing newly collated data on mouse spinal cord for direct comparisons. *Necab1/2* mRNA transcripts showed complementary distribution in rodent's spinal cord. Multiple-labeling fluorescence histochemistry with neuronal phenotypic markers localized NECAB1 to a dense fiber plexus in the dorsal horn, to neurons mainly in superficial layers and to commissural interneurons in both rodent species. NECAB1-positive (+) motor neurons were only found in mice. NECAB1 distribution in the human spinal cord was similar with the addition of NECAB1-like immunoreactivity surrounding myelinated axons. NECAB2 was mainly present in excitatory synaptic boutons in the dorsal horn of all three species, and often in calbindin-D28k$^+$ neuronal somata. Rodent ependymal cells expressed calbindin-D28k. In humans, they instead were NECAB2$^+$ and/or calretinin$^+$. Our results reveal that the association of NECAB2 to excitatory neuronal circuits in the spinal cord is evolutionarily conserved across the mammalian species investigated so far. In contrast, NECAB1 expression is more heterogeneous. Thus, our study suggests that the phenotypic segregation of NECAB1 and -2 to respective excitatory and inhibitory spinal systems can underpin functional modalities in determining the fidelity of synaptic neurotransmission and neuronal responsiveness, and might bear translational relevance to humans.

**Keywords** Calbindin-D28k · Ependymal cell · PKCγ · SST2A · VGLUT1 · VGLUT2

## Introduction

Calcium-binding proteins (CaBPs) can be divided into two subtypes: calcium *sensors* and calcium *buffers* (Burgoyne 2007; Schwaller 2010). One major cluster of CaBPs is

T. Harkany and T. Hökfelt shared senior authorship.

**Electronic supplementary material** The online version of this article (doi:10.1007/s00429-016-1191-3) contains supplementary material, which is available to authorized users.

✉ Ming-Dong Zhang
mingdong.zhang@ki.se

[1] Department of Neuroscience, Karolinska Institutet, 17177 Stockholm, Sweden

[2] Division of Molecular Neurobiology, Department of Medical Biochemistry and Biophysics, Karolinska Institutet, 17177 Stockholm, Sweden

[3] Department of Molecular Neurosciences, Center for Brain Research, Medical University of Vienna, Spitalgasse 4, 1090 Vienna, Austria

[4] Science for Life Laboratory, Department of Neuroscience, Karolinska Institutet, 17177 Stockholm, Sweden

[5] Department of Anatomy, Hokkaido University School of Medicine, 060-8638 Sapporo, Japan

[6] Institute of Ageing and Health, Newcastle University, Newcastle upon Tyne NE4 5PL, UK

[7] Department of Pharmaceutical Chemistry, Medical University of Vienna, 1090 Vienna, Austria

[8] Institute of Neurology, Medical University of Vienna, 1090 Vienna, Austria

[9] Science for Life Laboratory, Albanova University Center, Royal Institute of Technology, 10691 Stockholm, Sweden

within the EF-hand super-family whose members have variable repeats of conserved EF-hand motifs (Burgoyne 2007; Girard et al. 2015). For example, parvalbumin is a prototypic EF-hand calcium *buffer* which became prominent, particularly since it is a selective marker for GABA neurons in the central nervous system (Celio 1990; Antal et al. 1991; Andressen et al. 1993; Freund and Buzsaki 1996; Klausberger and Somogyi 2008). On the other hand, NCS-1 (neuronal $Ca^{2+}$ sensor-1), downstream regulatory element antagonistic modulator (DREAM) and secretagogin are calcium *sensors* with EF-hand motifs. They are, for example, present in primary somatosensory systems and likely involved in pain modulation (Cheng et al. 2002; Averill et al. 2004; Shi et al. 2012). However, there are still many predicted yet unstudied EF-hand CaBPs in the nervous system. Particularly, the dorsal root ganglia (DRGs) and spinal cord provide vast territories for future systems-level discoveries given the many modalities of neurons involved in sensory signaling.

Neuronal calcium-binding protein 1 and -2 (NECAB1 and -2) are CaBPs given their two N-terminal EF-hand motifs. NECAB1/2 were originally described as interacting targets for the presynaptic calcium *sensor* synaptotagmin I, as well as a down-stream target of Pax6 involved in the development of the mammalian retinal primordium, respectively (Bernier et al. 2001; Sugita et al. 2002; Sugita and Sudhof 2000). NECAB1-like immunoreactivity (LI) is, in the mouse brain, mainly restricted to subsets of neurons positioned distinctly in, e.g. layer 4 of the neocortex, striatum, hilus of the dentate gyrus, a wedge of pyramidal neurons in the CA2 subfield of the hippocampus, as well as subsets of thalamic, especially midline nuclei (e.g. mediodorsal, central medial, paraventricular and reuniens nuclei). NECAB1 expression was also found in the temporal lobe of the human brain (Wu et al. 2007). A recent in situ hybridization (ISH) study reported that NECAB1 $mRNA^{+}$ neurons are scattered throughout the mouse hippocampus, whereas the NECAB2 transcript is strongly expressed in CA2 pyramidal neurons (Zimmermann et al. 2013).

Both *Necab1* and *Necab2* mRNA transcripts are present in mouse DRG neurons, as shown by single-cell RNA sequencing (Usoskin et al. 2015; Li et al. 2015). Furthermore, NECAB2 is an identity marker for the subpopulation of neurofilament-containing DRG neurons and co-localizes with tyrosine kinase B receptor (Usoskin et al. 2015). Finally, a complete overview of the distribution of both two *Necab* transcripts in mouse brain and spinal cord is found in the Allen Brain Atlas based on digoxigenin labeled probes (Lein et al. 2007; Henry and Hohmann 2012).

During the past years, we have studied NECAB1/2 distribution at the spinal level. Our first report phenotyped DRG neurons and spinal cord in mouse (Zhang et al. 2014), allowing comparison with the published unbiased classification of sensory neuron types by large-scale single-cell RNA sequencing (Usoskin et al. 2015; Li et al. 2015) and the Allen Brain Atlas (Henry and Hohmann 2012). This study (Zhang et al. 2014) shows that both NECAB1/2 proteins are highly enriched in mouse DRG neurons, which mainly belong to the small and medium-sized populations. Moreover, in the spinal dorsal horn NECAB1/2 are to a large extent localized to glutamatergic excitatory interneurons.

The present study deals with NECAB1/2 mRNA and protein distribution in the rat and human spinal cord, which were analyzed on a backdrop of mouse data to provide direct comparisons. Yet we significantly extended this analysis by providing in situ hybridization (ISH) for both NECABs in all three species. We characterized NECAB1/2 neurons by ubiquitous, prototypic synapse markers, such as boutons (synaptophysin) (Wiedenmann and Franke 1985; Rehm et al. 1986; Navone et al. 1986), inhibitory systems (GAD67) (Erlander and Tobin 1991), excitatory neurotransmission (VGLUT1, VGLUT2) (Fremeau et al. 2004; Li et al. 2003; Kaneko et al. 2002) and protein kinase PKCγ (PKCγ) (Malmberg et al. 1997; Polgar et al. 1999; Mori et al. 1990); and somatostatin receptor 2A (SST2A) that labels superficial inhibitory interneurons both in mouse, rat and human (Shi et al. 2014; Polgar et al. 2013; Todd et al. 1998a, b). Finally, co-localization with calbindin-D28k and calretinin, both 'classical' calcium-binding proteins (Andressen et al. 1993), was also performed.

## Materials and methods

### Animals and human samples

Wild type male C57BL/6N mice ($n = 23$, adult, 12–14 weeks of age) and Sprague–Dawley rats ($n = 13$, adult, 250–300 g) were obtained from SCANBUR AB (Stockholm, Sweden). Mice and rats were kept under standard conditions on a 12/12 h-light/dark cycle with free access to food and water. Experiments complied with the Swedish policy for the use of research animals, and were approved by a local ethical committee (Stockholms Norra djurförsöksetiska nämnd N101/14). Efforts were made to minimize the number of animals used and their suffering throughout. Human spinal cord was obtained from a 48-year-old female subject who consented to and donated her organs for transplantation surgery (Regionala etikprövningsnämnden i Stockholm nämnd N98/035). Human hippocampal tissue was obtained from a 57-year-old male who passed away due to heart insufficiency (post-mortem delay ~8 h). No neurological symptoms were reported and neuropathological examination excluded

vascular or inflammatory lesions, neoplasms, or neurodegenerative diseases. Examination of the human tissue was performed in the frame of KIN-Neurobiobank (molecular neuropathological investigation of neurodegenerative diseases) and approved by the Ethical Committee of the Medical University of Vienna (N396/2011).

### Riboprobe synthesis for in situ hybridization

Antisense and sense RNA probes specific for *Necab1* and -*2* from mouse, rat and human were synthesized using sequence specific primers (Table S1). PCR fragments were subcloned into pCRII-TOPO vector (Invitrogen, Carlsbad, CA, USA) with their orientation confirmed by nucleotide sequencing (KIGene, Stockholm, Sweden). After linearization of the ensuing plasmid DNA, antisense and sense riboprobes were transcribed by T7/Sp6 RNA polymerase (Life Technologies, Carlsbad, CA, USA) in the presence of $^{35}$S-UTP (Perkin Elmer, Boston, MA, USA). Unincorporated nucleotides were removed on NucAway spin columns (Life Technologies). Sense probes were used as negative controls.

### In situ hybridization

For ISH, mice ($n = 5$) and rats ($n = 6$) were deeply anesthetized with sodium pentobarbital (50 mg/kg, i.p., APL, Stockholm, Sweden) and decapitated. Lumbar spinal cord segments were rapidly dissected, frozen on dry ice and sectioned on a CryoStar NX70 cryostat (Thermo Scientific, Walldorf, Germany) at 20-µm thickness. Sections were mounted onto Superfrost Plus microscope slides (VWR International, Leuven, Belgium) and stored at −80 °C. ISH was performed as described (Le Maitre et al. 2013). Briefly, tissue sections were postfixed in 4 % paraformaldehyde (PFA) and then treated with 0.25 % acetic anhydride in 0.1 M triethanolamine (pH 8.0). Sections were then dehydrated in graded alcohol and stored at −20 °C. Sections were pre-hybridized using 50 % (vol/vol) deionized formamide (pH 5), 50 mM Tris–HCl (pH 7.6), 25 mM EDTA (pH 8.0), 20 mM NaCl, 0.25 mg/ml, yeast tRNA and 2.5× Denhardt's solution for 4 h at 55 °C followed by hybridization in a humidified chamber overnight (14–16 h at 55 °C). Labeled probes were diluted to a final concentration of $1.0 \times 10^6$ cpm/200 µl in a solution containing 50 % (vol/vol) deionized formamide (pH 5.0), 0.3 M NaCl, 20 mM DTT, 0.5 mg/ml yeast tRNA, 0.1 mg/ml poly-A-RNA, 10 % (vol/vol) dextran sulfate, and 1× Denhardt's solution. After hybridization, sections were washed twice for 30 min in 1× SSC at 55 °C, 1 h in 50 % (vol/vol) formamide/0.5× SSC at 55 °C, 15 min in 1× SSC at 55 °C, 1 h in RNase A buffer at 37 °C, twice for 15 min in 1× SSC at 55 °C, dehydrated in an ascending series of ethanol (70, 90, 95, 100 %; 2 min each) and air-dried. Sections were first exposed to Kodak Biomax MR film (VWR International) and then dipped in an autoradiographic emulsion (Kodak, Rochester, NY, USA). After an 'individual' exposure time (2 weeks for mouse and rat *Necabs* and 8 weeks for human *Necabs*), slides were developed using D19 developer (Kodak) for 3 min and AL4 fixative (Kodak) for 7 min, dried at room temperature (RT, 22–24 °C), and then mounted with a medium containing 90 % glycerol/10 % PBS (vol/vol).

### Antibodies for immunohistochemistry

This comparative analysis was made possible by antisera cross-reacting with NECABs from the three species. As such, human *pr*otein *e*pitope *s*ignature *tag*s (PrESTs) showed >97 % identity with rodents (Fig. 1a). Anti-NECAB1/2 antibodies were generated by and obtained from Atlas Antibodies AB (Stockholm, Sweden). All antibodies used in this study (Table S2) have previously been extensively characterized, except the mouse monoclonal antibody against NECAB1 (same PrEST). However, the results with this monoclonal antibody reveal neural structures identical to those seen with the rabbit polyclonal antibody (Fig. S1). Thus, its use was amenable to successful double-labeling experiments.

### Immmunohistochemistry

For immunohistochemistry (IHC), mice ($n = 10$) and rats ($n = 5$) were deeply anesthetized with sodium pentobarbital and transcardially perfused with 4 % PFA in 0.16 M phosphate buffer (PB) as described previously (Shi et al. 2012). The lumbar 4 and 5 (L4, L5) segments of the spinal cord were dissected out and post-fixed in the same fixative for 90 min at 4 °C, followed by rinsing with 10 % sucrose in 0.1 M PB containing 0.01 % sodium azide (VWR International) and 0.02 % bacitracin (Sigma, St Louis, MO, USA). For the analysis of the human spinal cord, the tissue was immersion-fixed in 4 % PFA for 2 h and rinsed with 10 % sucrose in 0.1 M PB. Tissues were kept in 10 % sucrose solution (0.1 M PB) for at least 48 h at 4 °C. All trimmed tissues were embedded in OCT (HistoLab, Gothenburg, Sweden), frozen with liquid carbon dioxide and sectioned on a CryoStar NX70 cryostat (Thermo Scientific) at 20-µm thickness. The sections were mounted onto Superfrost Plus microscope slides (VWR International) and stored at −20 °C.

Mounted sections were air-dried at RT for at least 30 min and then incubated with select combinations of primary antibodies (Table S2) diluted in phosphate-buffered saline (PBS) containing 0.2 % (wt/vol) BSA (Sigma) and 0.3 % Triton X-100 (Sigma) in a humid chamber at

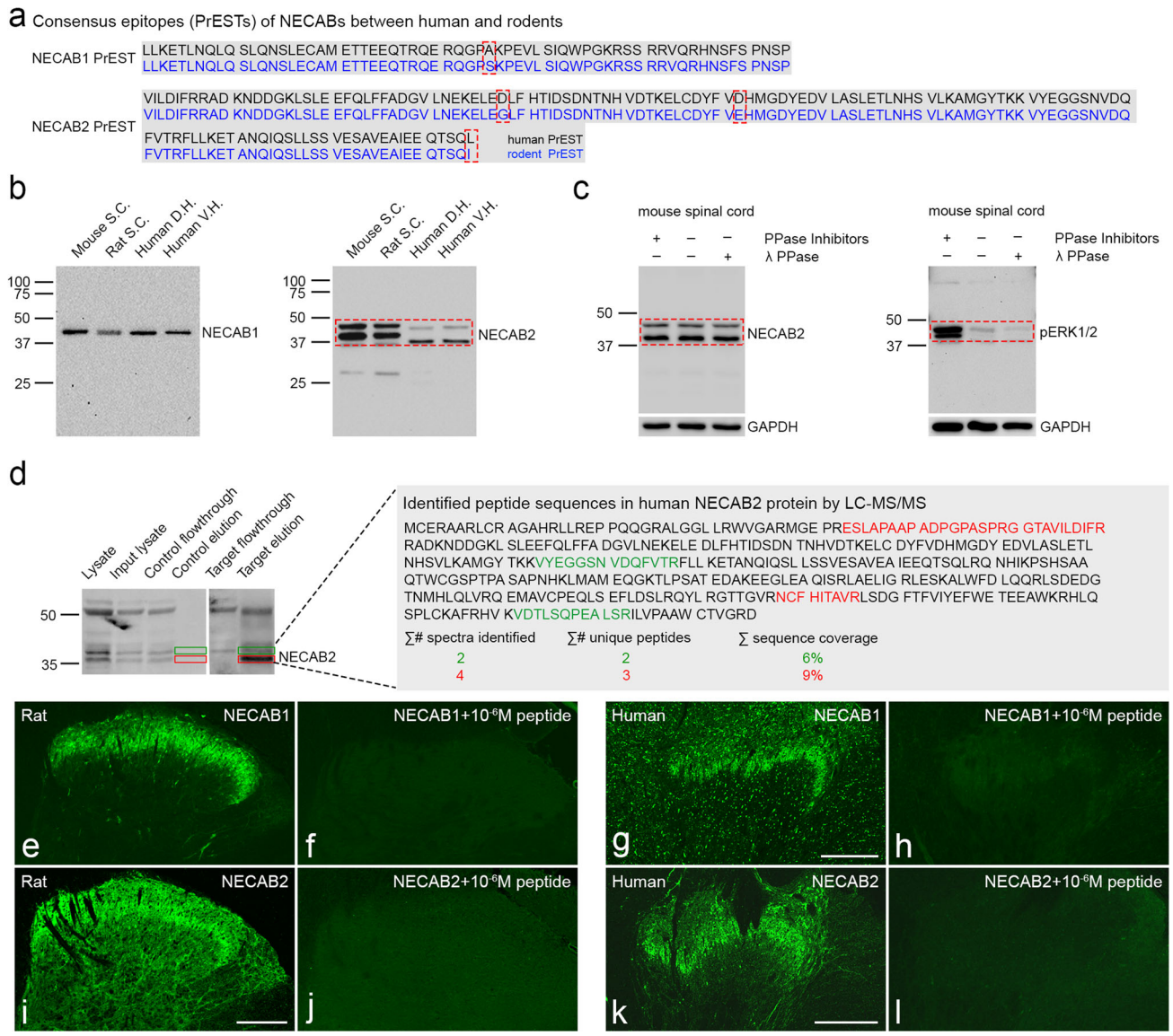


**Fig. 1** Western blotting and antigen adsorption experiments. **a** Comparison of human NECAB1- or 2 epitopes with corresponding fragments from rodents. The epitope similarity between human and rodents is more than 97 %. **b** Western blotting shows specific bands for NECAB1 and NECAB2 in spinal cord lysates from mouse, rat, and separated spinal dorsal and ventral lysates from human. **c** Lambda phosphatase treatment does not affect the NECAB2 band migration, whereas the bands for phospho-ERK1/2 cannot be detected after treatment. **d** Western blotting analysis reveals a specific signal (especially the shorter isoform) in eluted fraction of immunoprecipitation (IP) using an antibody against NECAB2 (target) compared to the elution in the control sample, where no antibody was used. Signal detected in the flowthrough of the control sample is comparable to that of the input lysate, while bands about 35 kDa seems to be almost completely precipitated by the target IP. In-gel digestion and LC–MS/MS analysis of proteins corresponding to signal detected by western blotting lead to the identification of NECAB2 from bands about 35 kDa in the target eluted fraction but not in the control eluted fraction (indicated by *green* and *red rectangles*). The protein is presented at least with two unique peptides in both target samples. Numbers of identified spectra, unique peptides and sequence coverage for NECAB2 are also summarized. **e–h** NECAB1-LI cannot be seen in rat and human spinal dorsal horn by adding $10^{-6}$ M PrEST of NECAB1 to the antibody solution. **i–l** The NECAB2-LI cannot be detected in rat and human spinal dorsal horn by adding $10^{-6}$ M PrEST of NECAB2 to the antibody solution. *Red dash rectangles* indicate specific bands for NECAB2 and pERK1/2 in **c** and **d**. *PrEST* protein epitope signature tag. *Scale bars* 200 μm in **e**, **f**, **i**, **j**, 500 μm in **g**, **h** and 500 μm in **k**, **l**

4 °C for 48 h. Immunoreactivities were visualized using the TSA Plus kit (PerkinElmer, Waltham, MA, USA) as previously described (Shi et al. 2012). For double- or triple-labeling, we performed double-'TSA Plus' staining (mouse monoclonal NECAB1 antibody combined with rabbit polyclonal PKCγ or SSTR2A antibody) or the indirect Coons procedure (Coons 1958) alone with mixed primary antibodies (NECAB2/VGLUT1/VGLUT2; NECAB2/VGLUT2/synaptophysin; NECAB2/calretinin/calbindin-D28k). Double-TSA plus staining was

performed as per (Brumovsky et al. 2007). Others were visualized with a mixture of secondary IgG (H + L) antibodies conjugated with Alexa Fluor488 (1:100), carbocyanin (Cy)3 or Cy5 (1:150, Jackson ImmunoResearch Laboratories, West Grove, PA, USA) (Zhang et al. 2014).

### Microscopy and image processing

Dark-field images of sections processed for in situ hybridization were captured on a Nikon microscope equipped with a Coolpix 5000 digital camera (Nikon, Tokyo, Japan). Representative photomicrographs of immunohistochemistry were acquired on an LSM700 confocal laser-scanning microscope (Zeiss, Jena, Germany) at 1 airy unit pinhole settings used uniformly for all images (Zhang et al. 2014). Emission spectra for each dye were limited as follows: DAPI (<480 nm), FITC/Alexa Fluro488 (505–540 nm), Cy3 (560–610 nm) and Cy5 (>640 nm). For co-localization analysis of presumed boutons (NECAB2/VGLUT1/VGLUT2; NECAB2/VGLUT2/synaptophysin; or NECAB2 with GAD67), images were acquired at 0.5-µm optical thickness with a 40× water objective (NA/1.40). In select cases, projection images were produced after orthogonal scanning (*z*-stack) using step-intervals of 1.0 µm (40 × 1.0). Images were processed using the ZEN2012 software (Zeiss). Multi-panel figures were assembled in Adobe Photoshop CS6 software (Adobe System, San Jose, CA, USA).

### Quantitative morphometry

The boundaries between laminae I, II and III were identified by observing myelin distribution (lack of myelin in lamina II), whereas the border between lamina II outer and inner layers was delineated by PKCγ-like immunoreactivity (PKCγ-LI, inner layer of lamina II) and of the neuropeptides galanin and calcitonin gene-related peptide (CGRP) (lamina I and outer layer of lamina II) (processed as described above) (Sardella et al. 2011; Hughes et al. 2003; Carlton et al. 1988). The laminar scheme of spinal cord was guided by the cytoarchitectonic organization of rat and human spinal cord (Molander et al. 1984; Haines 1987).

The quantification of co-localization between NECAB1$^+$ neurons and PKCγ$^+$ or SST2A$^+$ interneurons in superficial layers of the spinal dorsal horn performed on randomly acquired images (40× water objective, LSM700) according to the following criteria: laminae I and II of the mouse and rat spinal cord were covered from medial to lateral by 4–8 frames in a tile-scanning protocol (LSM700). We randomly acquired pictures from frames numbered with either odd or even descriptors (random table). Because of difficulties in distinguishing the punctate intracellular labeling of NECAB2$^+$ in the somata of interneuron from surrounding NECAB2$^+$ dendrites and boutons, the quantification of co-localization was only calculated as the percentage of PKCγ or SST2A expressing NECAB2 in the superficial layer. All co-localization data were expressed as mean ± standard deviation (SD) and transformed into percentages.

### Western blotting

For western blotting of NECAB1 and -2, mice ($n = 2$) and rats ($n = 2$) were deeply anesthetized with sodium pentobarbital and decapitated. Lumbar spinal cord segments were rapidly dissected, frozen on dry ice and stored at −80 °C until use. Human spinal cord was dissected, frozen and stored at −80 °C until use. Total protein was extracted from spinal cord by RIPA lysis buffer (50 mM Tris–HCl, pH 7.4, 1 % NP-40, 0.25 % sodium deoxycholate, 150 mM NaCl and 1 mM EDTA) also containing a protease inhibitor cocktail (P8340, Sigma). For phosphorylation modification, spinal cord samples from mice ($n = 4$) were extracted with RIPA lysis buffer as above and spinal cord samples ($n = 2$) with RIPA lysis buffer containing phosphatase inhibitors (1 mM NaF and 1 mM $Na_3VO_4$) as controls. Lambda protein phosphatase treatment performed according to manufacture's instructions (New England Biolabs, Hitchin, UK). Western blotting was performed according to previous published protocols (Zhang et al. 2014).

Briefly, boiled samples (95 °C for 5 min) with loading buffer were separated on 10 % SDS-PAGE gels, transferred onto polyvinylidine fluoride (PVDF) membranes, and blocked with 5 % non-fat dry milk in TBS (Tris-buffered saline) with 0.1 % Tween-20 for 1 h at RT, and incubated with an antibody against NECAB1 or -2 (anti-rabbit, 1:5000 in 5 % BSA; Atlas Antibodies AB) or phospho-ERK1/2 (Thr202/Tyr204, anti-rabbit, 1:5000 in 5 % BSA; CellSignaling Technology, Danvers, MA, USA) for 48 h at 4 °C. After incubation with HRP-conjugated secondary antibodies (1:5000–1:10,000, DAKO, Glostrup, Denmark) and exposed to ECL (GE Healthcare, Buckinghamshire, UK), membranes were scanned on a ChemiDOC$^{TM}$ + Imaging system (Bio-Rad Laboratories, Hercules, CA, USA). Membranes were stripped and re-probed with anti-GAPDH antibody (anti-rabbit, 1:1000 in 5 % BSA, CellSignaling Technology) used as the loading control.

### Immunoprecipitation

Protein G agarose beads (Pierce/Thermo Fisher Scientific, Rockford, IL, USA) were incubated with 1.5 µg antibody against NECAB2 (HPA013998) for 2 h at 4 °C. Beads

were washed and further incubated with 150 µl human hippocampal lysate (1 µg/µl) for 4 h. Following intense washing, proteins were eluted by incubation with reducing loading buffer (Amersham WB System, GE Healthcare, Uppsala, Sweden) at 95 °C for 5 min. To monitor immunoprecipitation (IP) efficiency, a flow-through fraction was collected after the incubation of the tissue lysate with antibody-coupled beads. As control, the above protocol was conducted without antibody. Fractions were separated by SDS-PAGE (Amersham) and probed for NECAB2. Electrophoresis and western blotting were performed according to manufacturer's instructions, similar to the above description of western blotting. Membranes were developed with goat anti-rabbit Cy3-conjugated secondary antibodies (1:1000 in 3 % BSA in TBS, Amersham).

### In-gel digestion and LC–MS/MS analysis

Next, we repeated the above immunoprecipitation protocol for NECAB2, including SDS-PAGE. Bands, corresponding to those revealed by immunoreactivity in western blotting, were excised and proteins were in-gel digested with sequencing grade modified Trypsin (Promega, Madison, WI, USA) as reported (Ghafari et al. 2015).

Liquid chromatography–tandem mass spectrometry (LC–MS/MS) was performed on an Ultimate 3000 nano RSLC system (Thermo Fisher Scientific, Sunnyvale, CA, USA) coupled to an amaZon Speed ETD ion trap mass spectrometer (Bruker Daltonics, Bremen, Germany) via a CaptiveSpray ion source. Data were acquired using Hystar 3.2 (Bruker Daltonics). Peptide samples were loaded onto a trap column (300 µm ID × 5 mm, packed with Acclaim PepMap100 C18, 5 µm, 100A, Thermo Fisher Scientific) at a flow rate of 30 µl/min for 4 min using 0.1 % formic acid (FA). After washing, the peptides were back-flushed to and separated on a 25 cm analytical column packed with C18 reversed phase material (75 µm ID, packed with Acclaim PepMap RSLC C18, 2 µm, 100A, Thermo Fisher Scientific) at a constant flow rate of 300 nl/min. HPLC solvents were 0.1 % FA in water (solvent A) and 0.08 % FA in 80 % acetonitrile (solvent B). Peptides were eluted with a 11 min gradient ranging from 4 to 13 % solvent B, followed by a 85 min gradient from 13 to 35 % solvent B and finally with a 1 min gradient from 35 to 96 % solvent B. Eluted peptides were analyzed in a data-dependent acquisition mode using a collision-induced dissociation method. In each peptide scan, maximum 10 precursor ions were selected for $MS^2$ above the intensity threshold of 25,000 with the dynamic exclusion of 0.20 min. MS spectra were acquired in positive mode in a scan range of 400–1400 *m/z* and the scan range for MS/MS was always scaled to the precursor. SPS tune was set to 900 *m/z*. ICC target and maximum accumulation time were determined as 400,000 and 50 ms for MS and 500,000 and 100 ms for MS/MS. Isolation width was 2.2 *m/z* and fragmentation cutoff was set to 20 % with 60 % fragmentation amplitude using the Enhanced SmartFrag option from 80 to 120 % in 30 ms.

Raw data were interpreted using Compass DataAnalysis 4.1 (Bruker Daltonics) and proteins were identified using the Mascot search engine (Matrix Science, London, UK). Spectra were matched against the Swiss-Prot human (*Homo sapiens*) reference proteome database (as of November 2015; 20,187 entries). The MS/MS ion search parameters were the following: the number of maximum missed cleavages for trypsin was 2; peptide mass tolerance was ±0.35 Da (# $^{13}$C=1) and fragment mass tolerance was ±0.4 Da; carbamidomethylation of cysteine residues and oxidation of methionine residues were determined as fixed and variable modifications, respectively. Significant threshold for matched peptides was given as $p < 0.05$. Protein identity was considered as verified, if it was present at least with two unique peptide sequences (Sase et al. 2015).

## Results

### Methodological considerations: specificity of NECAB1 and NECAB2 antibodies

NECAB1 and -2 are encoded by 13 exons, highly conserved in mouse, rat and human. Our Western blotting results demonstrated a high degree of similarity at the protein level (molecular mass) using lysates from the spinal cord of the three species (Fig. 1b). NECAB1 was visualized as a single band around 41 kDa uniformly for mouse, rat and human (Fig. 1b). In contrast, NECAB2 appeared as two bands at around 39 and 43 kDa, corresponding to its two isoforms predicted for mouse and rat. In human spinal cord, NECAB2 was detected as two bands, but with a considerable smaller mass as compared to mouse and rat (Fig. 1b). Migration difference between rodents and human was not caused by modified phosphorylation (Fig. 1c). Similarly, a migration shift for NECAB2 also occurred in human hippocampus (Fig. 1d). Notably, unique peptides fragments identical to amino acid sequences in NECAB2 could be identified by LC–MS/MS from both immunoreactive bands (Fig. 1d; Fig. S2). These observations support that, despite their size variation in human tissues, antibodies raised against NECAB2 recognize their predicted cognate target and are thus specific.

Additional adsorption experiments using immunizing peptides (so called PrESTs) as baits showed the lack of NECAB1- and NECAB2-LI in rat and human spinal cord after pre-incubation of the antisera (Fig. 1e–l), as previously shown for mouse (Zhang et al. 2014). Moreover,

parallel analysis with mouse monoclonal and rabbit polyclonal anti-NECAB1 antibodies in human spinal cord revealed similar results (Fig. S1).

In ISH studies, none of the labeling with antisense riboprobes was seen after hybridization with sense probes (insets in Fig. 2a, g, m, Fig. 2r; insets in Fig. 5g, m; Fig. 5r). Thus, an apparent precise overlap between ISH and IHC results with regards to cell body localization further support specificity.

### Distribution of *Necab1* mRNA transcripts

In the mouse spinal cord, the *Necab1* mRNA transcripts were extensively expressed in neurons in the first two (superficial) layers, with very few cells in lamina III (Fig. 2a, b). Scattered, intensely labeled neurons were also observed in the lateral deep layers (laminae IV and V) (Fig. 2a, c). Positive neurons were found in layer X, mainly dorsal to the central canal, and extended laterally (Fig. 2a, d, e). Furthermore, motor neurons in lamina IX of spinal ventral horn were densely labeled (Fig. 2a, f). *Necab1* in the rat spinal cord showed a similar distribution, with the exception that motor neurons could not be detected (Fig. 2g–l). The results from the human spinal cord are less clear (Fig. 2m). Only single neurons could be identified in the dorsal horn, e.g. in lateral lamina II (Fig. 2n), and in deep layers (lamina IV/V) (Fig. 2o), whereas several distinctly labeled neurons in lamina X surrounded the central canal in the human cord (Fig. 2p, q).

### Distribution of NECAB1 protein

Overall, the cellular distribution of NECAB1 protein was similar to that of the *Necab1* mRNA transcript, although being more abundant and distinct in the human spinal cord. Thus, the NECAB1 antiserum intensely labeled neurons and fiber networks in various parts of the spinal cord from both rodents, including the superficial layers, lateral lamina V, lamina X and lamina VII/VIII, as shown in cross sections of spinal cord from mouse and rat (Fig. 3a, f). Many neurons in the superficial layers were NECAB1$^+$ (Fig. 3b, g). Relatively large NECAB1-immunoreactive (IR) neurons with long processes were located in lateral lamina V bordering the white matter (Fig. 3c, h). There were patches of NECAB1-IR neurons located above the central canal in lamina X (Fig. 3d, i). In mouse spinal ventral horn, NECAB1-IR commissural interneurons were located in its medial aspects with long processes extending towards the mid-line (Fig. 3e). Similar NECAB1-IR neurons were also observed in lamina VII/VIII of the rat (Fig. 3j). However, NECAB1-IR motor neurons were observed in mouse (indicated by dashed magenta circle in Fig. 3a) but not in rat (Fig. 3f). In human spinal cord, the NECAB1 staining was indistinct when viewed at low-power, but a fluorescent band could still be seen in lamina II, as well as evenly distributed small rings, also in the spinal white matter (Figs. 1g, 3k). At higher resolution, clearly labeled neurons were seen in superficial layers, including neurons in the lateral lamina II (Fig. 3l), lamina V (Fig. 3m) and lamina X (Fig. 3n). Both polyclonal and monoclonal anti-NECAB1 antibodies labeled round structures surrounding myelinated axons; in fact, a fluorescent band of varying thickness could be seen around most axons (Fig. 3o). Importantly, this, as all other staining, was eliminated by antigen pre-adsorption (Fig. 1g, h). Taken together, the distribution pattern of NECAB1, both with regards to its mRNA transcript and protein, is similar in mouse and rat, an exception being the lack of NECAB1-IR motor neurons in rat and of periaxonal rings in both rodents species.

### NECAB1 co-localization with PKCγ or SST2A

SST2A is a conserved neurochemical marker for inhibitory interneurons in the spinal dorsal horn, present both in rodents and human. PKCγ is a conserved marker specific for excitatory interneurons in inner layer of lamima II, and also labels the corticospinal tract, the anatomical localization of which however is different between rodents and human (Fig. S3a–e). In the mouse, only few (2.5 ± 0.7 %) NECAB1-IR neuron profiles (NPs) were SSTR2A$^+$. Conversely, 15.3 ± 2.3 % of SSTR2A-IR NPs were NECAB1$^+$ (Fig. 4a). In the rat, 11.1 ± 3.5 % of the NECAB1-IR NPs were SSTR2A$^+$ in the superficial layers, and the proportion of SSTR2A-IR neurons expressing NECAB1 was 54.0 ± 7.4 % (Fig. 4b). Very few NECAB1-IR NPs were PKCγ$^+$ in the mouse superficial dorsal horn (1.3 ± 1.0 %) and less than 10 % of the PKCγ-IR NPs were NECAB1$^+$ (6.8 ± 6.7 %), the latter always being weakly labeled (Fig. 4c). However, in rat 12.1 ± 0.6 % of the NECAB1-IR neurons were PKCγ$^+$ and half of the PKCγ-IR NPs were NECAB1$^+$ (55.4 ± 0.7 %), distinctly contrasting mouse (cf. Fig. 4c, d). Taken together, mouse and rat show distinct differences with regard to the neurochemical heterogeneity of NECAB1$^+$ neurons in superficial dorsal horn.

### Distribution of *Necab2* mRNA transcripts

In mouse spinal cord, *Necab2* mRNA transcripts were abundant in inner lamina II (lamina IIi) and extended into lamina III, with only scattered cells in lamina I and outer lamina II (lamina IIo, Fig. 5a, b). *Necab2* mRNA was also detected in the deep layers (Fig. 5a, c), including lamina X (Fig. 5d) and the ventral horn (Fig. 5e), but was excluded

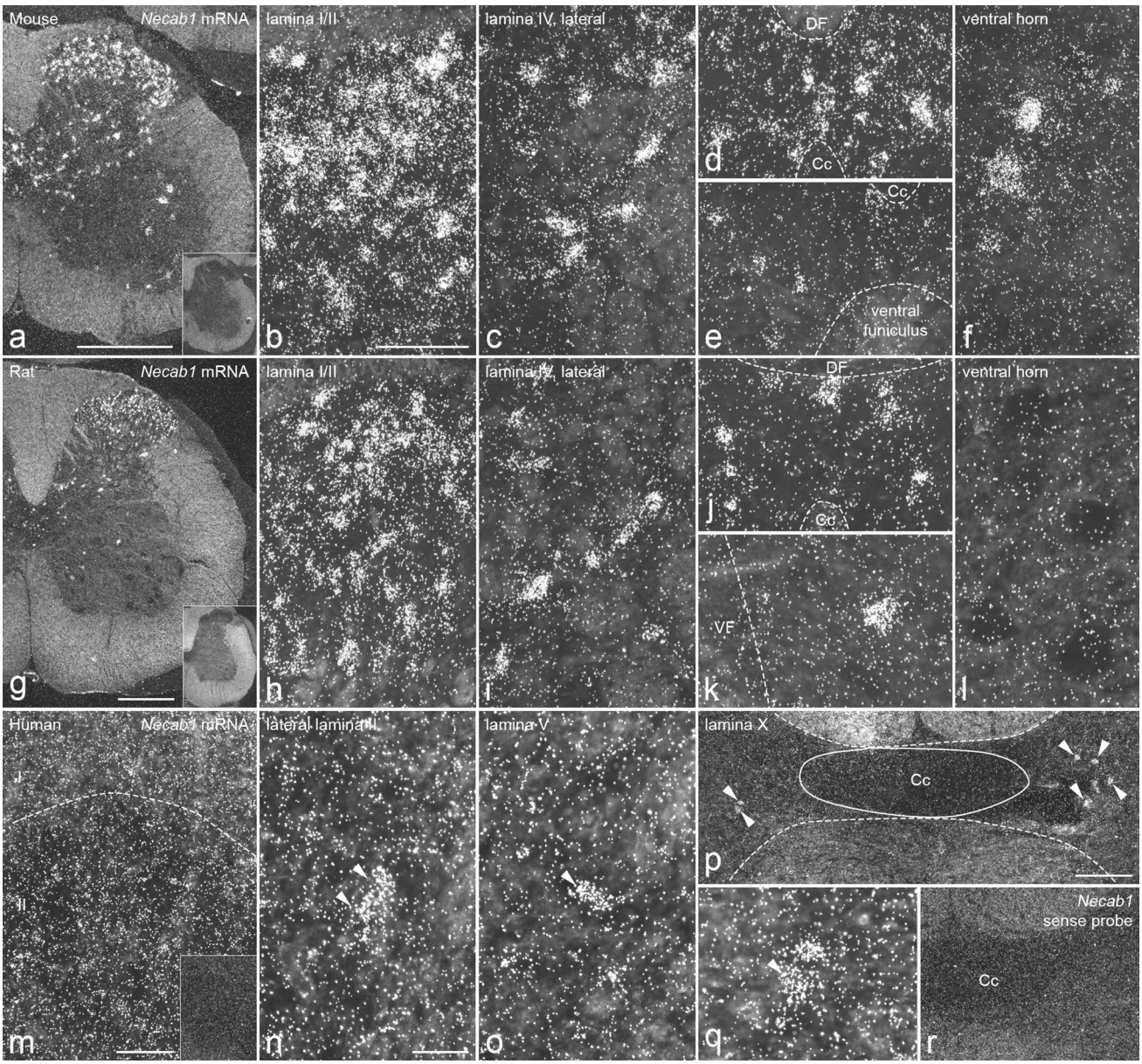


**Fig. 2** *Necab1* mRNA distribution in mouse, rat and human spinal cord. **a** Overview of *Necab1* transcripts labeled by $^{35}$S in dark field from mouse lumbar spinal cord. The inset shows the sense probe of mouse *Necab1*. **b–f** *Necab1* transcripts are abundant in superficial layers, deep layers, lamina X and motor neurons in the ventral horn. **g** Overview of *Necab1* transcripts labeled by $^{35}$S in dark field from rat lumbar spinal cord. The *inset* shows the sense probe of rat *Necab1*. **h–l** *Necab1* transcripts are abundant in superficial layers, also in scattered neurons from deep layers, areas surrounding lamina X but not motor neurons in the ventral horn. **m** Overview of *Necab1* transcripts labeled by $^{35}$S in dark field from human lumbar spinal dorsal horn. It is hard to identify *Necab1*$^{+}$ neurons in spinal superficial layers. **n**, **o** A few neurons with abundant *Necab1* transcripts are found in lateral lamina II and deep layers i.e. lamina V. **p**, **q** Neurons in lateral area of lamina X are frequently labeled by *Necab1* probe. The *Necab1* sense probe does not show any specific labeling spinal dorsal horn (*inset* in **m**) or central canal (**r**). *Arrowheads* indicate the positive neurons (**n–q**) and (*dashed*) *lines* indicate the borders (**d**, **e**, **j**, **k**, **m**, **p**). *DF* dorsal funiculus, *VF* ventral funiculus, *Cc* central canal. *Scale bars* 500 μm in **a**, **g**, 100 μm in **b–f**, **h–l**, 100 μm in **m**, 50 μm in **n**, **o**, **q**, 250 μm in **p**, **r**

from motor neurons (Fig. 5f). In rat, *Necab2* mRNA transcripts were found in all layers (Fig. 5g–l), including single motor neurons (Fig. 5g, l). In the human dorsal horn, scattered small, *Necab2* mRNA-containing cells were distributed within a narrow band along the border between lamina IIi and lamina III (Fig. 5m, n), as well as in lamina I and lamina IV (Fig. 5m, o). In addition, *Necab2* mRNA was found in many ependymal cells lining the central canal and in cell bodies surrounding the central canal (lamina X) (Fig. 5p, q).

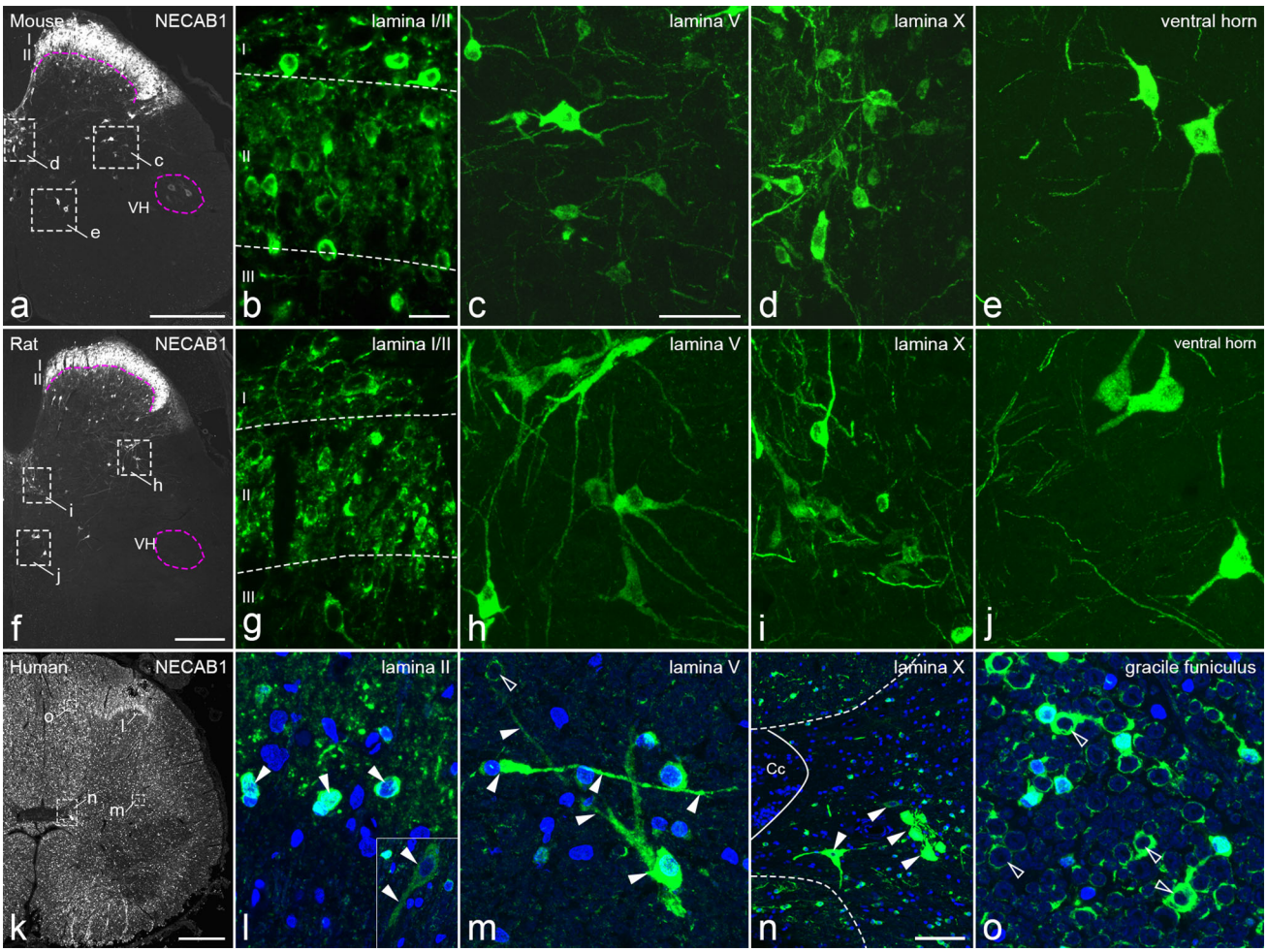


**Fig. 3** Expression of NECAB1 in mouse, rat and human spinal cord. **a** Overview of NECAB1-like immunoreactivity (LI) in mouse lumbar spinal cord. **b–e** High magnification of NECAB1-IR neurons (indicated by *dashed rectangles* in **a**) in superficial layers, lateral spinal cord of deep layers, areas between central canal and dorsal funiculus or ventral funiculus. **f** Overview of NECAB1-LI in rat lumbar spinal cord. **g–j** High magnification of NECAB1-IR neurons (indicated by *dashed rectangles* in **f**) in superficial layers, lateral spinal cord of deep layers, lamina X (between central canal and dorsal funiculus) and lamina VII/VIII along ventral funiculus. *Dashed magenta lines* indicate the border between lamina II and lamina III. *Dashed magenta ovals* in ventral horn from **a** and **f** highlight the areas of motor neurons. **k** Overview of NECAB1-LI in human spinal cord. **l–n** High magnification of NECAB1-IR neurons (indicated by *arrowheads*) from lamina II (**l**), lateral lamina V (**m**) and lamina X (**n**). **o** NECAB1-LI is abundant in white matter of spinal cord i.e. the gracile funiculus. DAPI (*blue*) is used to show the nuclei in **l–o**. The *open arrowheads* indicate the NECAB1-IR cells without nucleus (**m**), especially in gracile funiculus (**o**). *White dashed lines* show the borders of spinal lamination in **b**, **g** and **n** (border of central canal is labeled by *full curved line*). *Scale bars* 200 μm in **a**, **f**, 1 mm in **k**, 20 μm in **b**, **g**, **l**, **o**, 50 μm in **c–e**, **h–j**, **m**, 100 μm in **n**

## Distribution of NECAB2 protein

NECAB2 primarily stained bouton-like structures throughout the spinal cord, with neuronal somata more moderately stained in the dorsal horn. Even though this pattern was relatively conserved between rodents and human, particularly in the dorsal horn, key differences exist (Fig. 6a, f, k): NECAB2-LI showed the strongest signal in lamina IIi in all species. Yet it extended into lamina III in mouse (Fig. 6a, b), whereas it intruded into lamina I with a sharp border between lamina II and III in rat and human (Fig. 6f, g, k, l). Bouton (punctate) staining was seen in all species, with highest density in laminae I-II. The boutons were larger in the human spinal cord. In deep spinal layers of rat and human (laminae III–V), distinctly labeled NECAB2-IR neurons were observed, whereas in mouse they were more diffusely distributed (cf. Fig. 6c, d, h, i, m, n). In the ventral horn, NECAB2-IR punctate staining with different intensity was observed in all species (human > mouse > rat), and some NECAB2-IR neurons occasionally occurred in rat ventral horn (Fig. 6e, j, o). NECAB2-LI was observed within the human central canal, not seen in either mouse or rat (Fig. 6a, f, k) (see below).

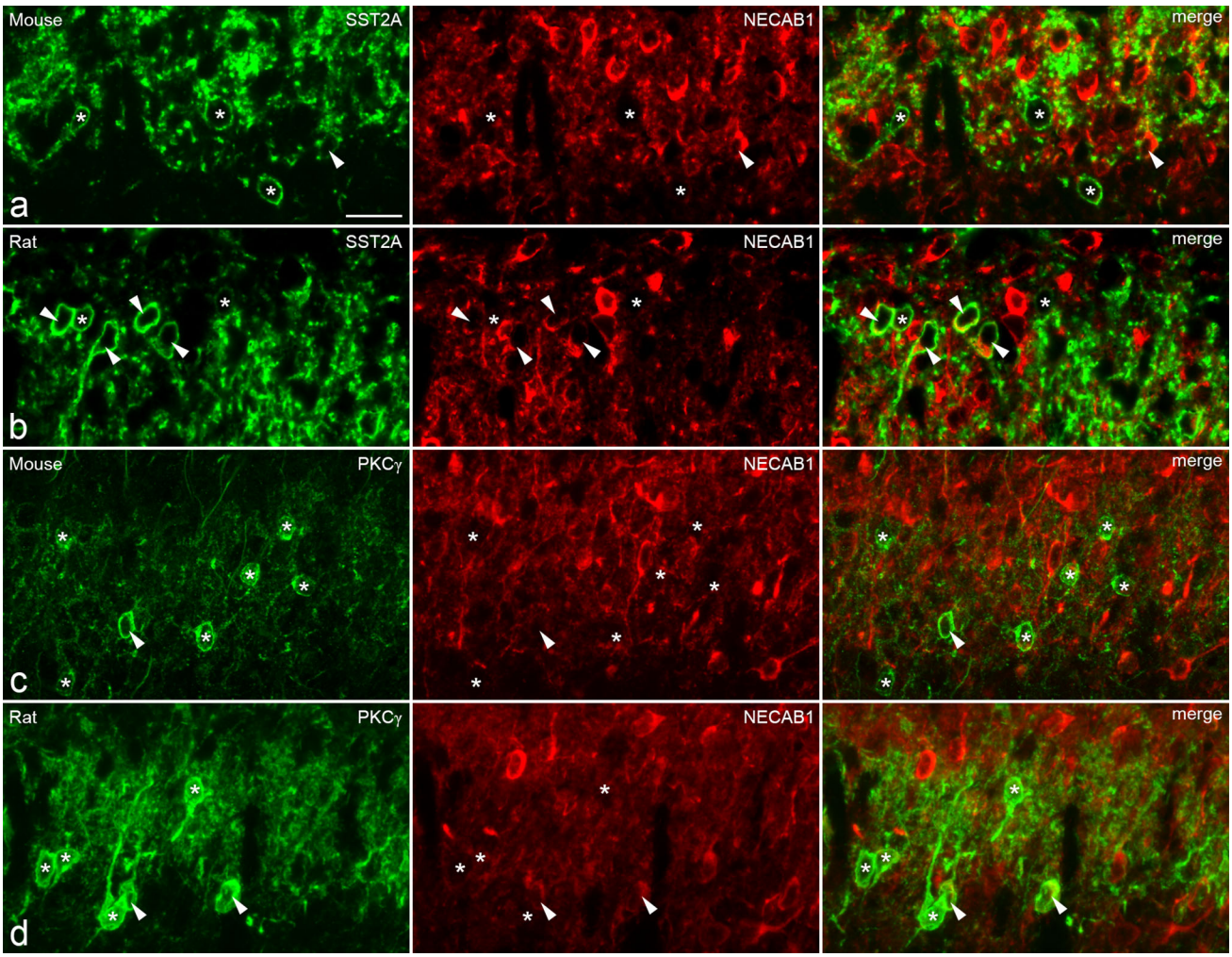


**Fig. 4** Co-localization of NECAB1 with SST2A or PKCγ. **a** High magnification pictures show double labeling between SST2A (*green*) and NECAB1 (*red*) in mouse superficial layers. **b** High magnification pictures show double labeling for SST2A and NECAB1 in rat superficial layers. *Asterisks* indicate $SST2A^+$ neurons but NECAB1 negative, whereas *arrowheads* indicate co-localized ones in **a** and **b**. **c** High magnification pictures show double labeling for PKCγ (*green*) and NECAB1 (*red*) in mouse lamina IIi. **d** High magnification pictures show double labeling for PKCγ and NECAB1 in rat lamina IIi. Projection pictures in **c** and **d** are produced from 5 μm *z*-stack scanning. *Asterisks* indicate $PKC\gamma^+$ neurons but NECAB1 negative, whereas *arrowheads* indicate co-localized neurons in **c** and **d**. *Scale bars* 20 μm

## NECAB2 co-localization with SST2A, GAD67 or PKCγ

In mouse spinal cord, only few (7.5 ± 5.5 %) SSTR2A-IR NPs were $NECAB2^+$ in the superficial layers (Fig. 7a). In rat spinal cord, 18.0 ± 7.8 % of the SSTR2A-IR NPs were $NECAB2^+$, but they were usually only weakly labeled (Fig. 7b). In human dorsal horn, only few $SSTR2A^+$ neuronal somata were detected, and none was NECAB2-IR. However, some NECAB2-IR puncta co-localized with SSTR2A (Fig. 7c).

Coexistence of NECAB2-IR and GAD67 was not detected in boutons, neither in mouse/rat nor human spinal cord (Fig. 7d–f). Occasionally, $GAD67^+$ puncta formed basket-like structures around $NECAB2^+$ boutons (inset in Fig. 7f). Only few GAD67-IR cell bodies were detected, but they did not co-localize with NECAB2 in any of the three species. Furthermore, double-labeling experiments showed that most PKCγ-IR interneurons were $NECAB2^+$ in lamina II of mouse (95.4 ± 2.1 %, Fig. 8a), and this was similar in rat (89.3 ± 1.2 %, Fig. 8b). However, in human dorsal horn the percentage of $NECAB2^+$ PKCγ-IR NPs was lower (46.9 %, Fig. 8c).

## NECAB2 mainly coexists with $VGLUT2^+$ in $synaptophysin^+$ boutons

To further establish that the punctate structures are nerve endings of excitatory nature, we performed triple labeling of NECAB2 with VGLUT1 and -2, or with synaptophysin and VGLUT2. First, a conserved overlapping distribution

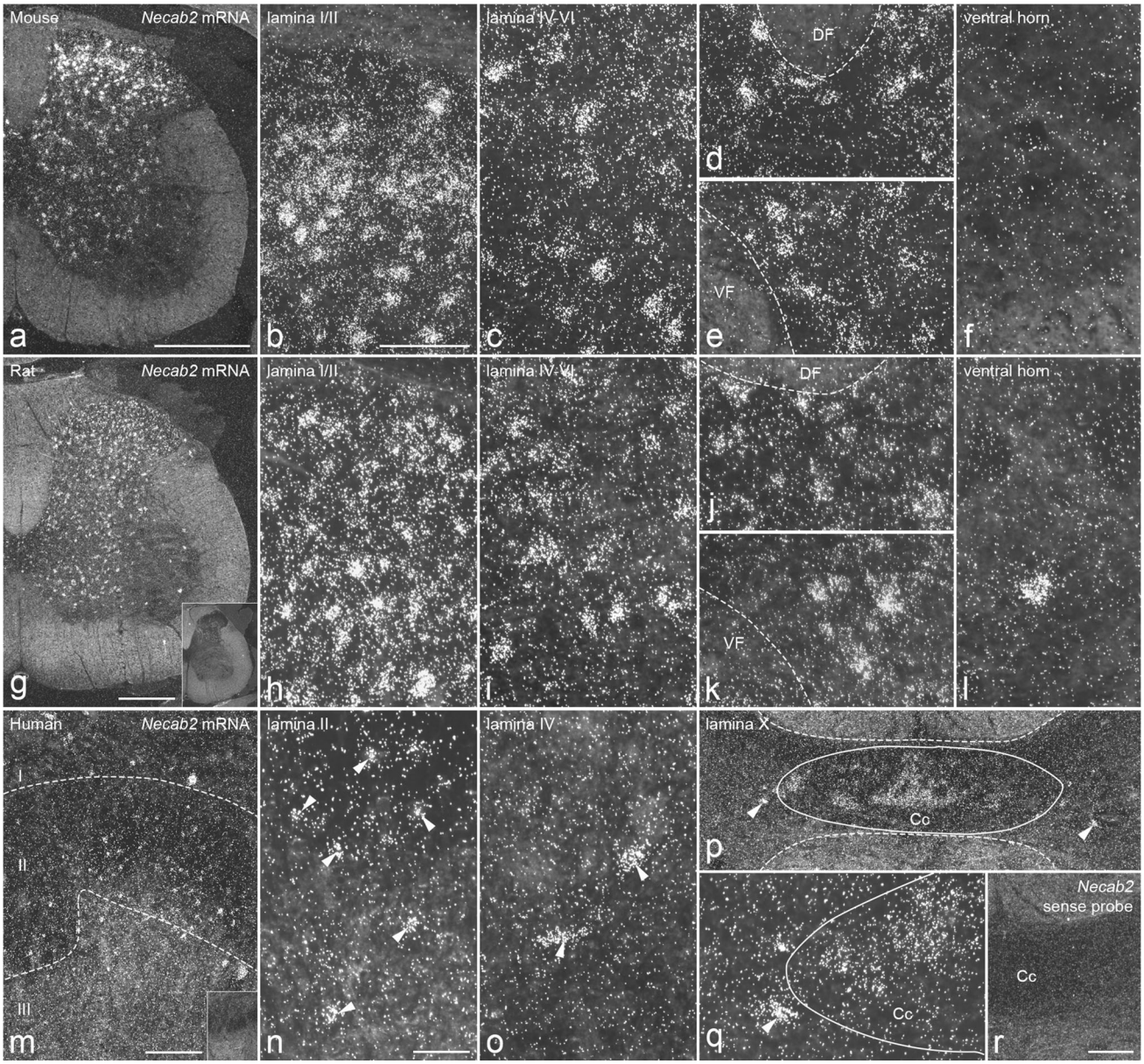


**Fig. 5** *Necab2* mRNA distribution in mouse, rat and human spinal cord. **a** Overview of *Necab2* transcripts labeled by $^{35}S$ in dark field from mouse lumbar spinal cord. **b–f** *Necab2* transcripts are abundant in lamina IIi (extending into lamina I and III), also in deep layers, areas surrounding lamina X, but not in motor neurons in the ventral horn. **g** Overview of *Necab2* transcripts labeled by $^{35}S$ in dark field from rat lumbar spinal cord. The *inset* shows the sense probe of rat *Necab2*. **h–l** *Necab2* transcripts are homogeneously distributed through the spinal cord, but relatively weaker in the area with motor neurons. **m** Overview of *Necab2* transcripts labeled by $^{35}S$ in dark field from human lumbar spinal dorsal horn (lamina I–III). **n–q** *Necab2* transcripts are distributed the narrow band between lamina IIi and lamina III, with scattered neurons in lamina IV, lamina X and ependymal cells around the central canal. The *Necab2* sense probe does not show any specific labeling in the spinal dorsal horn (*inset* in **m**) or around the central canal (**r**). *Arrowheads* indicate the positive neurons and *dashed lines* indicate the borders of spinal lamination. Central canal is indicated by *curved lines* in **p** and **q**. *Scale bars* 500 μm in **a** and **g**, 100 μm in **b–f** and **h–l**, 200 μm in **m**, **p**, **r**, 50 μm in **n**, **o**, **q**

pattern of VGLUT1 and VGLUT2 was demonstrated in mouse, rat and human (Fig. S4a–f). The dense labeling of VGLUT1 (laminae III–IV and spinal ventral horn) and VGLUT2 (lamina I–II, lateral spinal cord of deep layers, and area surrounding central canal) was complementary (Fig. S4a–f). In mouse, NECAB2-IR boutons extensively co-localized with VGLUT2, and some of them (NECAB2$^+$/VGLUT2$^+$) were also VGLUT1$^+$ (Fig. 9a, a1–a4), and many synaptophysin$^+$ (Fig. 9b, b1–b4). In rat NECAB2-IR boutons also co-localized with VGLUT2 and rarely with VGLUT1 (Fig. 9c, c1–c4); and many of them (NECAB2$^+$/VGLUT2$^+$) were also synaptophysin$^+$ (Fig. 9d, d1–d4), as in mouse (Fig. 9b4). In human spinal cord, many VGLUT1-IR boutons were VGLUT2$^+$, but NECAB2-LI only co-

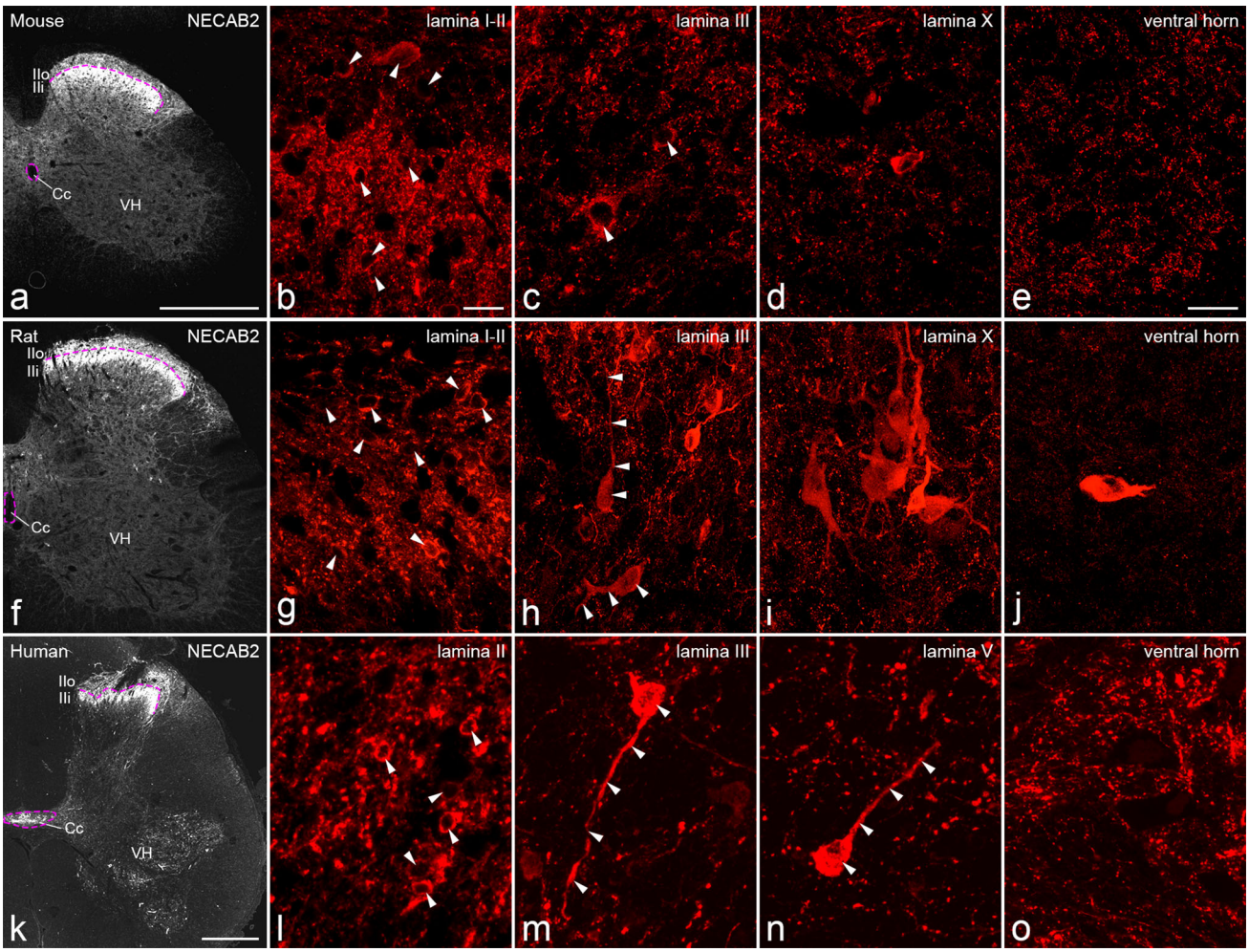


**Fig. 6** Expression of NECAB2 in mouse, rat and human spinal cord. **a** Overview of NECAB2-LI in mouse lumbar spinal cord. **b–e** High magnification pictures show NECAB2-IR neurons (indicated by *arrowheads*) and boutons in superficial layers, deep layers, lamina X and lamina IX of ventral horn (areas with motor neurons). **f** Overview of NECAB2-LI in rat lumbar spinal cord. **g–j** High magnification pictures show NECAB2-IR neurons and boutons in superficial layers, deep layers, lamina X (area between central canal and dorsal funiculus) and lamina VII of spinal ventral horn. **h–j** Pictures are projected from *z*-stack scanning (13, 16 and 20 µm, respectively). **k** Overview of NECAB2-LI in human lumbar spinal cord. **l–o** High magnification pictures show NECAB2-IR neurons and boutons in superficial layers, deep layers (lamina III and V), and lamina VI/VII of spinal ventral horn. **m**, **n** Pictures are projected from 13 µm *z*-stack scanning. *Dashed magenta lines* indicate the border between lamina IIo and lamina IIi in **a**, **f** and **k**. Central canals were labeled by *dashed magenta ovals* in **a**, **f** and **k**. *Cc* central canal, *VH* ventral horn. *Scale bars* 500 µm in **a**, **f** 1 mm in **k**, 20 µm in **b–d**, **g–j** and **l–n**, 50 µm in **e**, **o**

localized with VGLUT2 (Fig. 9e, e1–e4). Similar to mouse and rat, NECAB2$^+$/VGLUT2$^+$ boutons largely co-localized with synaptophysin (Fig. 9f, f1–f4).

## Similar distribution of calretinin, calbindin-D28k and NECAB2 in the dorsal horn

Previously, we have described the distribution and co-localization of NECAB2 with calretinin or calbindin-D28k in the mouse dorsal horn (Zhang et al. 2014). Here, we expanded this analysis to rat and human. The overview of

**Fig. 7** Co-localization of NECAB2 with SST2A or GAD67. **a–c** ▶ High magnification pictures show double labeling for SST2A (*green*) and NECAB2 (*red*) in mouse, rat and human superficial layers. *Asterisks* indicate SST2A$^+$ neurons but NECAB2 negative, *arrows* indicate the opposite situation, and *arrowheads* indicate the co-localized neurons in **a–c**. *Open arrowheads* indicate co-localized SST2A and NECAB2 terminals in **c**. **d–f** High magnification pictures show the double labeling for GAD67 (*red*) and NECAB2 (*blue*) in spinal lamina IIi from mouse, rat and human, respectively. The *insets* show boutons positive for NECAB2, but negative for GAD67. *Asterisks* indicate GAD67$^+$ neurons but NECAB2 negative neurons, *arrows* indicate NECAB2$^+$ but GAD67-negative neurons in **d–f**. *Scale bars* 20 µm in **a–c**, 10 µm in **d**, **e**, 10 µm in **f**

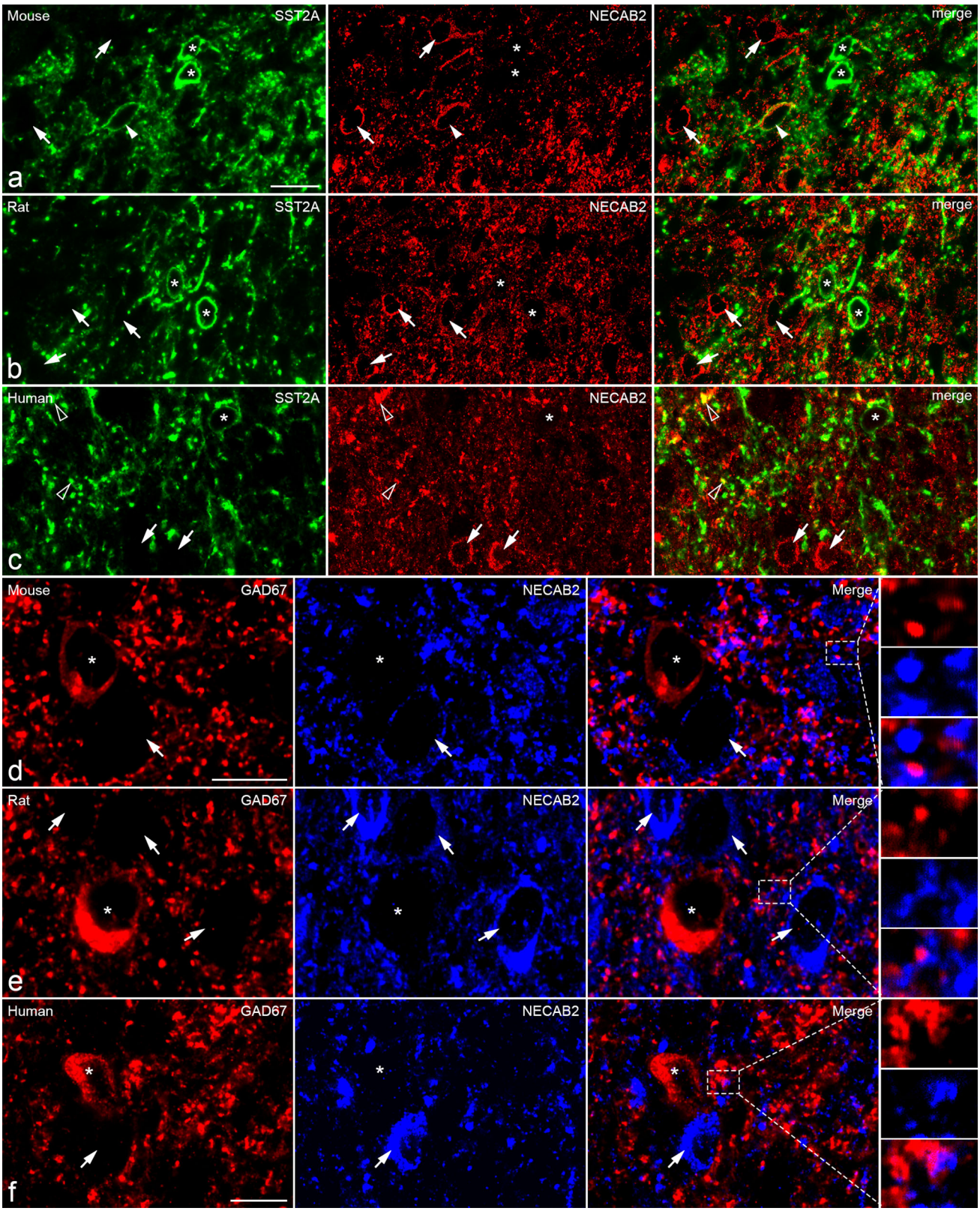
Mouse
SST2A
NECAB2
merge
a
Rat
SST2A
NECAB2
merge
b
Human
SST2A
NECAB2
merge
c
Mouse
GAD67
NECAB2
Merge
d
Rat
GAD67
NECAB2
Merge
e
Human
GAD67
NECAB2
Merge
f

calretinin or calbindin-D28k staining in spinal cord from mouse, rat and human shows similar patterns (Fig. 10), except for the lack of expression for calretinin and calbindin-D28k around the central canal (Fig. S5a–f). In mouse, NECAB2-IR neurons in the inner part of lamina II were largely calbindin-D28k$^+$ and some of them also calretinin$^+$ (Fig. 10a, a1–a4), with a similar distribution pattern of NECAB2 and calbindin-D28k in rat. Both of them extensively labeled the inner part of lamina II, with a clear border between lamina II and III (Fig. 10b), which was different from that of mouse (Fig. 10a). In lamina IIi, NECAB2-IR interneurons highly co-localized calbindin-D28k and many of them were also positive for calretinin (Fig. 10b, b1–b4). In human, the distribution of NECAB2 and calbindin-D28k was similar to mouse, possibly even more so with rat (Fig. 10c). In human lamina II, NECAB2-IR interneurons extensively co-localized calbindin-D28k and some of them also calretinin (Fig. 10c, c1–c4).

### Calcium-binding proteins in ependymal cells

The expression of calretinin-, calbindin-D28k- and NECAB2-LIs was different in ependymal cells along the central canal. Calbindin-D28k-LI, but not calretinin or NECAB2, was observed in mouse and rat ependymal cells (Fig. 11a, b). However, a 'switch' was seen in human. Thus, calretinin (sparse) and NECAB2 (abundant) were expressed in human ependymal cells, whereas calbindin-D28k could not be detected (Fig. 11c). Instead, neurons in lamina X (surrounding the central canal) expressed calretinin, calbindin-D28k and NECAB2 in the human cord (Fig. 11c, c1–c4). The counter staining with cresyl violet confirmed structural difference, showing well-organized ependymal cells along the central lumen in rodents and a hypocellular layer mixed with ependymal cells, but without lumen in human (Fig. 11d–f).

## Discussion

The present results demonstrate an overall anatomical distribution of NECAB1 and -2 in mouse, rat and human spinal cord. A previous study of mouse was entirely based on immunohistochemistry (Zhang et al. 2014), but here we, in addition to throughout newly acquired immunofluorescence images on mouse, include results of the transcripts using ISH, in this way providing further evidence on the

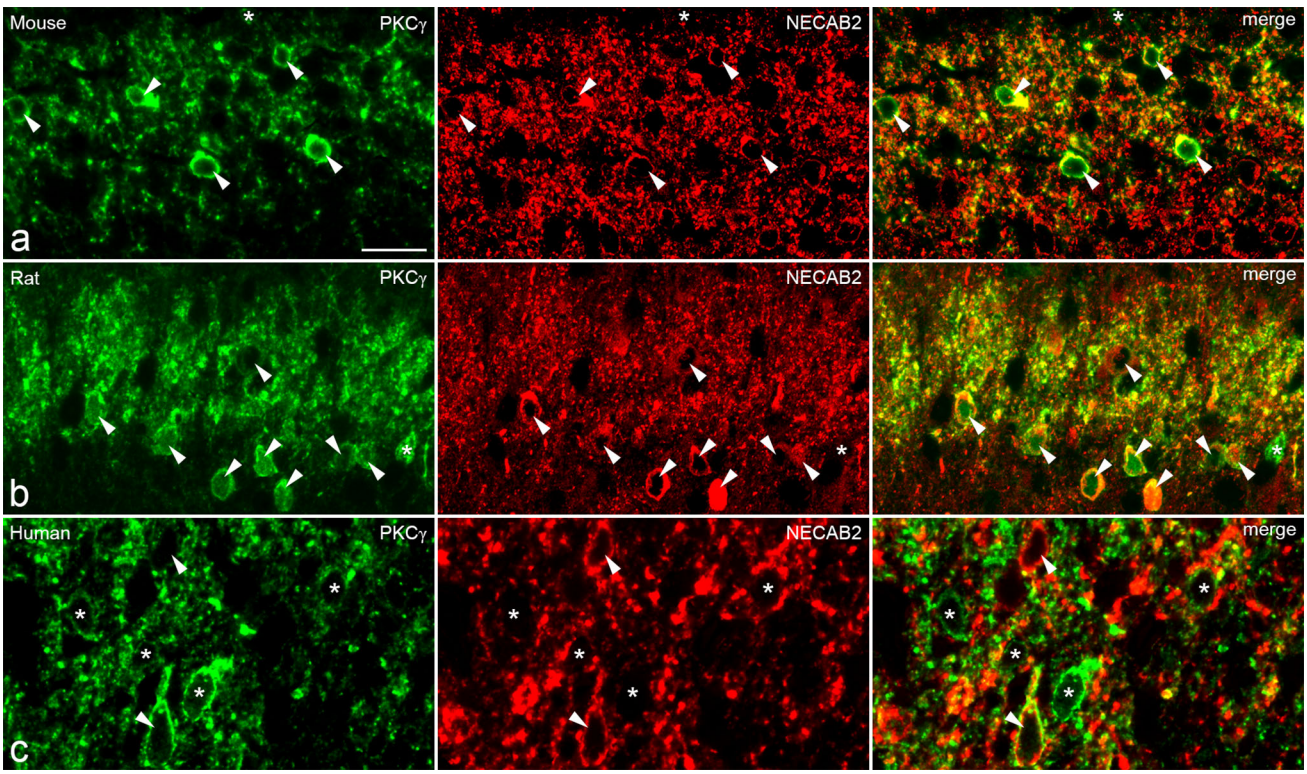


**Fig. 8** Co-localization of NECAB2 with PKCγ. **a** High magnification pictures show double labeling for PKCγ (*green*) and NECAB2 (*red*) in mouse spinal lamina IIi. **b** High magnification pictures show double labeling for PKCγ (*green*) and NECAB2 (*red*) in rat spinal lamina IIi. Projection pictures in **b** are produced from 5 µm *z*-stack scanning. **c** High magnification pictures show double labeling for PKCγ (*green*) and NECAB2 (*red*) in human spinal lamina IIi. *Asterisks* indicate PKCγ$^+$ but NECAB2 negative neurons, whereas *arrowheads* indicate co-localized ones in **a**–**c**. *Scale bars* 20 µm

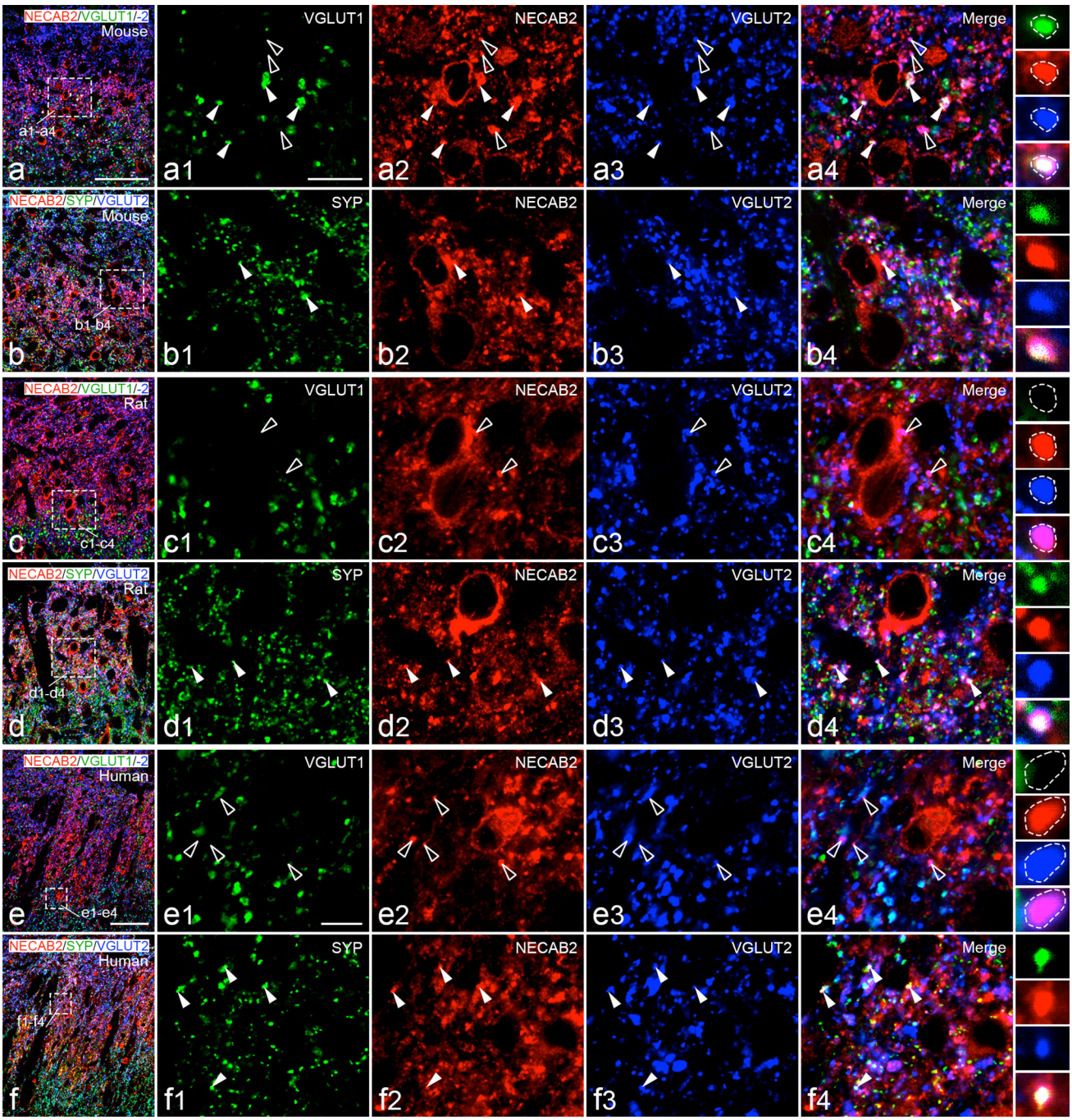


**Fig. 9** Conserved distribution of NECAB2 in excitatory boutons. **a**, **c**, **e** Overview of triple labeling of NECAB2 (*red*) with VGLUT1 (*green*) and VGLUT2 (*blue*) in spinal dorsal horn (lamina I–III) from mouse, rat and human, respectively. High magnification pictures show boutons in the inset in lamina IIi from **a** in **a1**–**a4**, from **c** in **c1**–**c4** and from **e** in **e1**–**e4**. *Filled arrowheads* indicate the boutons positive for NECAB2, VGLUT1 and VGLUT2, whereas *open arrowheads* indicate boutons positive for NECAB2 and VGLUT2 but negative for VGLUT1. Single punctate staining is presented at the end of the *panel* and surrounded by *dashed lines* to show the difference between mouse, rat and human (**a**, **c**, **e**). **b**, **d**, **f** Overview of triple labeling of NECAB2 (*red*) with SYP (*green*) and VGLUT2 (*blue*) in spinal dorsal horn (lamina I–III) from mouse, rat and human, respectively. High magnification pictures show boutons in the *inset* in lamina IIi from **b** in **b1**–**b4**, from **d** in **d1**–**d4** and from **f** in **f1**–**f4**. *Filled arrowheads* indicate the boutons positive for NECAB2, SYP and VGLUT2. Single punctate staining is presented at the end of the *panel* (**b**, **d**, **f**) to show the co-localization. *Scale bars* 50 μm in **a**–**d**, 10 μm in **a1**–**a4**, **b1**–**b4**, **c1**–**c4** and **d1**–**d4**, 100 μm in **e**, **f**, 10 μm in **e1**–**e4** and **f1**–**f4**

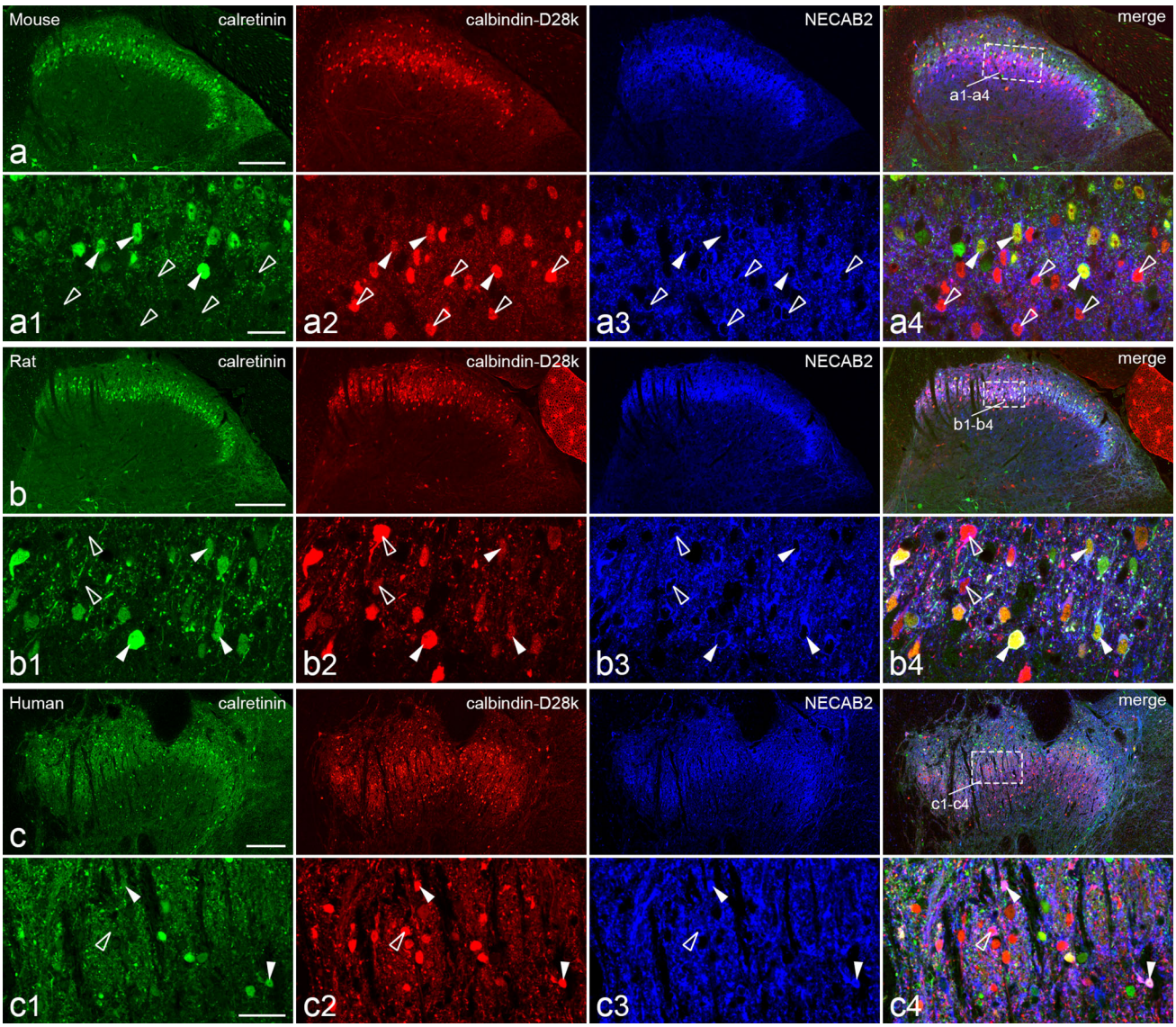


**Fig. 10** Co-localization of NECAB2 with calretinin and calbindin-D28k. **a–c** Overview of triple labeling of NECAB2 (*blue*) with calretinin (*green*) and calbindin-D28k (*red*) in spinal dorsal horn from mouse, rat and human, respectively. **a1–a4**, **b1–b4**, **c1–c4** High magnification pictures show co-localization in neuronal cell bodies in lamina II from *insets* in **a–c**. *Filled arrowheads* indicate the neuronal cell bodies positive for NECAB2, calretinin and calbindin-D28k, whereas *open arrowheads* indicate neurons positive for NECAB2 and calbindin-D28k but negative for calretinin. *Scale bars* 100 μm in **a**, 200 μm in **b**, 500 μm in **c**, 20 μm in **a1–a4**, **b1–b4**, 50 μm in **c1–c4**

specificity of the distribution patterns presented. An important finding is that in all three species NACAB2 is found in nerve endings, that is close to the site of synaptic signaling, a rare feature of CaBPs, including NECAB1.

## Similar anatomical distribution but diverse neurochemical profiles for NECAB1

NECAB1 expression in mouse spinal cord, including the commissural interneuron system, is nearly perfectly re-represented in rat, except for an apparent lack of NECAB1 in motor neurons at both the mRNA and protein levels. The NECAB1$^+$ commissural interneurons in mouse (Zhang et al. 2014) and rat lamina VII/VIII may originate from ventral V3 interneurons. They are primarily located in lamina VIII and act as premotor neurons to synchronize motor outputs (Borowska et al. 2013). NECAB1 represents a candidate marker for this subset of commissural interneurons involved in coordinating left/right locomotion (Kiehn 2011; Talpalar et al. 2013; Borgius et al. 2014; Birinyi et al. 2003).

The SST2A receptor, a conserved neurochemical marker for inhibitory interneurons in spinal superficial layers (Polgar et al. 2013; Todd et al. 1998b), is involved in the

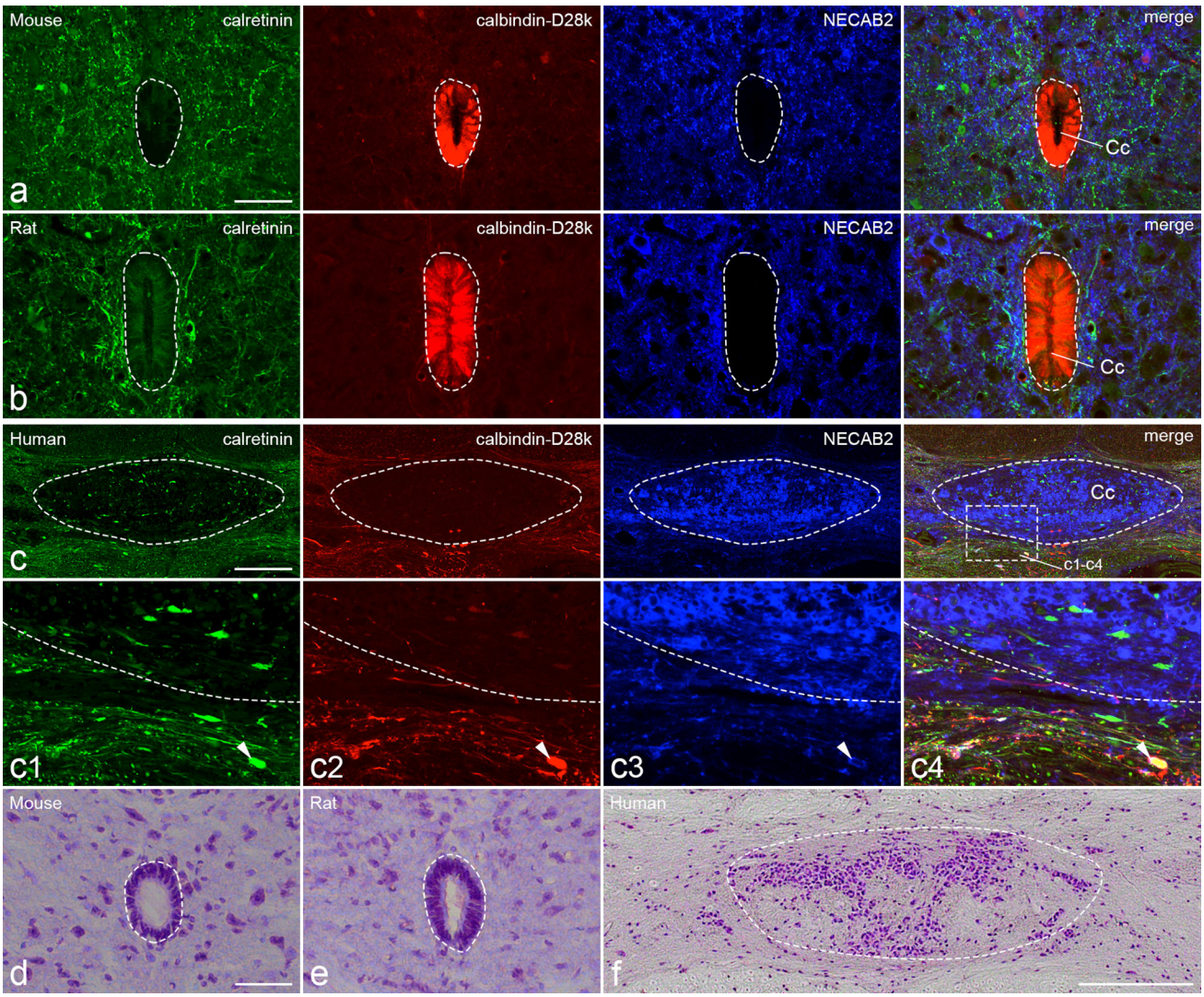


**Fig. 11** Expression of NECAB2, calretinin or calbindin-D28k in ependymal cells of spinal central canal. **a–c** Overview of triple labeling of NECAB2 (*blue*) with calretinin (*green*) and calbindin-D28k (*red*) in ependymal cells of spinal central canal from mouse, rat and human, respectively. The central canal is outlined by *dashed line*. The *arrowhead* in **c1–c4** indicated a neuron in lamina X (under the central canal) is positive for NECAB2, calretinin and calbindin-D28k. **d–f** Pictures of cresyl violet counter staining in central canal from mouse, rat and human, respectively. The central canal is indicated by *dashed line*. *Scale bars* 50 μm in **a**, **b**, **c1–c4**, 200 μm in **c**, 50 μm in **d**, **e**, 200 μm in **f**

development of neuropathic pain and itch (Shi et al. 2014; Polgar et al. 2013). In our present study, NECAB1 is expressed in half of the rat SST2A$^+$ interneurons, but in mouse only very few SST2A$^+$ interneurons are NECAB1$^+$. These observations corroborate our previous findings on the NECAB1 population in mouse having excitatory properties (Zhang et al. 2014). PKCγ labels a small subset of excitatory lamina IIi interneurons involved in pain modulation in both mouse and rat spinal cord. In fact, half of the PKCγ$^+$ neurons in rat are NECAB1$^+$, contrasting the situation in mouse (only a few, weakly labeled ones were co-localized). Taken together, NECAB1 is in rat expressed both in excitatory and inhibitory neurons in the spinal superficial layers, vs. virtually only in excitatory ones in mouse.

## Distribution and conserved excitatory profile of NECAB2

The anatomical distribution of NECAB2 in spinal dorsal horn, especially the strong labeling in lamina IIi, is conserved from rodents to human. However, the *Necab2* mRNA transcripts were found across the spinal cord, with a much wider distribution than seen for cell bodies using IHC. This may be due to an underestimation as a consequence of a rapid centrifugal transport of the NECAB2

protein, precluding detection in the neuronal soma. This is a well-known phenomenon in IHC studies on neuropeptides (e.g. Ljungdahl et al. 1978), and more recently for vesicular glutamate transporters (VGLUTs) (e.g. Hajszan et al. 2004) and presynaptic 7-transmembrane receptors (e.g. Stanic et al. 2006). An alternative explanation is of course lack of protein translation from pre-existing mRNA.

Some differences are encountered at the mRNA level, showing that *Necab2* mRNA has a more limited distribution in human than in rodents. However, we still cannot rule out the possibility that also this transcript is widely expressed in human spinal cord, like in rodents, since the sensitivity of the probe may not be optimal and since the quality of the human spinal cord labeling may be case-dependent, and of a lower quality compared to rodent spinal cord.

NECAB2 expression in excitatory presynaptic boutons is evidenced by its co-localization with VGLUT1/2 and synaptophysin, but not with GAD67, in all three species—the co-localization with VGLUT2 being particularly extensive. VGLUT2 is an accepted and main marker for excitatory glutamatergic interneurons in rodent and human spinal cord (and elsewhere) (Zhang et al. 2014; Oliveira et al. 2003; Malet et al. 2013; Todd et al. 2003; Landry et al. 2004). This has also been documented in functional studies, including experiments with knock-out mice, demonstrating the involvement of VGLUT2 in nocifensive behavior and spontaneous and pruritogen-evoked scratching (Scherrer et al. 2010; Lagerstrom et al. 2010; Liu et al. 2010; Moechars et al. 2006).

### NECAB2 in ependymal cells in rodents vs. human

Ependymal cells in the lesioned adult spinal cord are the source of astrocytes and participate in scar formation to inhibit further neuronal degeneration after spinal cord injury (Johansson et al. 1999; Sabelstrom et al. 2013; Lang et al. 2004; Barnabe-Heider et al. 2010). Earlier work has demonstrated the presence of calbindin-D28k, but not calretinin, in ependymal cells around the rodent central canal (Ren and Ruda 1994). Here, we confirm these findings and add that rodent ependymal cells do not express either of the two NECABs. However, many ependymal cells located within the human central canal were NECAB2$^{+}$ and a small number also calretinin$^{+}$/NECAB2-negative. Thus, interestingly, human ependymal cells are not well 'organized' but occupy the lumen, contrasting the regular pseudostratified, ciliated epithelium seen in rodents. However, in the human infant spinal cord ependymal cells are lining a fully open central canal, (Alfaro-Cervello et al. 2014; Milhorat et al. 1994). The central canal as observed here could be morphologically classified as ependymal rosette groups (Yasui et al. 1999; Milhorat et al. 1994). This occluded central canal develops with aging but may occur as early as in the 20s (Milhorat et al. 1994; Kasantikul et al. 1979; Yasui et al. 1999; Garcia-Ovejero et al. 2015). Furthermore, Alfaro-Cervello et al. (2014) have recently proposed that the stenosed adult human central canal is characterized by a hypocellular layer between ependymal cells, very much unlike the case in rodents. This new view is supported by an MRI study (Garcia-Ovejero et al. 2015). Taken together, the important role of ependymal cells in ameliorating spinal cord injury in adult rodents may suggest that NECAB2 (and calretinin) in ependymal cells within the human central canal represent an interesting target for further studies of lesions at the spinal level.

**Acknowledgments** Support for this study was provided by the Swedish Medical Research Council (T.Hö., T.Ha.), Karolinska Institutet, partial financing of graduate student funds (M.-D.Z., T.Ha., and T.Hö.); funding from the Karolinska Institutet (T.Hö., T.Ha.), the Novo Nordisk Foundation (T.Ha. and T.Hö.), the Swedish Brain Foundation (T.Ha. and T.Hö.), the Augusta and Petrus Hedlund Foundation (T.Ha. and T.Hö.) and the European Commission's PAINCAGE 7th Framework Programme (T.Ha. and T.Hö.). Laser-scanning microscopy was made available by the Center for Live Imaging of Cells (CLICK) at Karolinska Institutet, an imaging core facility supported by the Knut and Alice Wallenberg Foundation.

**Compliance with ethical standards**

**Conflict of interest** The authors declare no conflicts of interest.

## References

Alfaro-Cervello C, Cebrian-Silla A, Soriano-Navarro M, Garcia-Tarraga P, Matias-Guiu J, Gomez-Pinedo U, Molina Aguilar P, Alvarez-Buylla A, Luquin MR, Garcia-Verdugo JM (2014) The adult macaque spinal cord central canal zone contains proliferative cells and closely resembles the human. J Comp Neurol 522(8):1800–1817. doi:10.1002/cne.23501

Andressen C, Blumcke I, Celio MR (1993) Calcium-binding proteins: selective markers of nerve cells. Cell Tissue Res 271(2):181–208

Antal M, Polgar E, Chalmers J, Minson JB, Llewellyn-Smith I, Heizmann CW, Somogyi P (1991) Different populations of parvalbumin- and calbindin-D28k-immunoreactive neurons contain GABA and accumulate 3H-D-aspartate in the dorsal horn of the rat spinal cord. J Comp Neurol 314(1):114–124. doi:10.1002/cne.903140111

Averill S, Robson LG, Jeromin A, Priestley JV (2004) Neuronal calcium sensor-1 is expressed by dorsal root ganglion cells, is axonally transported to central and peripheral terminals, and is concentrated at nodes. Neuroscience 123(2):419–427

Barnabe-Heider F, Goritz C, Sabelstrom H, Takebayashi H, Pfrieger FW, Meletis K, Frisen J (2010) Origin of new glial cells in intact and injured adult spinal cord. Cell Stem Cell 7(4):470–482. doi:10.1016/j.stem.2010.07.014

Bernier G, Vukovich W, Neidhardt L, Herrmann BG, Gruss P (2001) Isolation and characterization of a downstream target of Pax6 in the mammalian retinal primordium. Development 128(20):3987–3994

Birinyi A, Viszokay K, Weber I, Kiehn O, Antal M (2003) Synaptic targets of commissural interneurons in the lumbar spinal cord of neonatal rats. J Comp Neurol 461(4):429–440. doi:10.1002/cne.10696

Borgius L, Nishimaru H, Caldeira V, Kunugise Y, Low P, Reig R, Itohara S, Iwasato T, Kiehn O (2014) Spinal glutamatergic neurons defined by EphA4 signaling are essential components of normal locomotor circuits. J Neurosci 34(11):3841–3853. doi:10.1523/JNEUROSCI.4992-13.2014

Borowska J, Jones CT, Zhang H, Blacklaws J, Goulding M, Zhang Y (2013) Functional subpopulations of V3 interneurons in the mature mouse spinal cord. J Neurosci 33(47):18553–18565. doi:10.1523/JNEUROSCI.2005-13.2013

Brumovsky P, Watanabe M, Hokfelt T (2007) Expression of the vesicular glutamate transporters-1 and -2 in adult mouse dorsal root ganglia and spinal cord and their regulation by nerve injury. Neuroscience 147(2):469–490. doi:10.1016/J.Neuroscience.02.068

Burgoyne RD (2007) Neuronal calcium sensor proteins: generating diversity in neuronal $Ca^{2+}$ signalling. Nat Rev Neurosci 8(3):182–193. doi:10.1038/nrn2093

Carlton SM, McNeill DL, Chung K, Coggeshall RE (1988) Organization of calcitonin gene-related peptide-immunoreactive terminals in the primate dorsal horn. J Comp Neurol 276(4):527–536. doi:10.1002/cne.902760407

Celio MR (1990) Calbindin D-28k and parvalbumin in the rat nervous system. Neuroscience 35(2):375–475

Cheng HY, Pitcher GM, Laviolette SR, Whishaw IQ, Tong KI, Kockeritz LK, Wada T, Joza NA, Crackower M, Goncalves J, Sarosi I, Woodgett JR, Oliveira-dos-Santos AJ, Ikura M, van der Kooy D, Salter MW, Penninger JM (2002) DREAM is a critical transcriptional repressor for pain modulation. Cell 108(1):31–43

Coons AH (1958) Fluorescent antibody methods. In: Danielli JF (ed) General cytochemical methods. Academic Press, New York, pp 399–422

Erlander MG, Tobin AJ (1991) The structural and functional heterogeneity of glutamic acid decarboxylase: a review. Neurochem Res 16(3):215–226

Fremeau RT Jr, Voglmaier S, Seal RP, Edwards RH (2004) VGLUTs define subsets of excitatory neurons and suggest novel roles for glutamate. Trends Neurosci 27(2):98–103. doi:10.1016/j.tins.2003.11.005

Freund TF, Buzsaki G (1996) Interneurons of the hippocampus. Hippocampus 6(4):347–470. doi:10.1002/(SICI)1098-1063(1996)6:4<347:AID-HIPO1>3.0.CO;2-I

Garcia-Ovejero D, Arevalo-Martin A, Paniagua-Torija B, Florensa-Vila J, Ferrer I, Grassner L, Molina-Holgado E (2015) The ependymal region of the adult human spinal cord differs from other species and shows ependymoma-like features. Brain 138(Pt 6):1583–1597. doi:10.1093/brain/awv089

Ghafari M, Whittle N, Miklosi AG, Kotlowski C, Schmuckermair C, Berger J, Bennett KL, Singewald N, Lubec G (2015) Dietary magnesium restriction reduces amygdala-hypothalamic GluN1 receptor complex levels in mice. Brain Struct Funct 220(4):2209–2221. doi:10.1007/s00429-014-0779-8

Girard F, Venail J, Schwaller B, Celio MR (2015) The EF-hand Ca(2+)-binding protein super-family: a genome-wide analysis of gene expression patterns in the adult mouse brain. Neuroscience 294:116–155. doi:10.1016/j.neuroscience.2015.02.018

Haines DE (1987) Neuroanatomy: an atlas of structures, sections, and systems, 2nd edn. Urban and Schwarzenberg, Baltimore

Hajszan T, Alreja M, Leranth C (2004) Intrinsic vesicular glutamate transporter 2-immunoreactive input to septohippocampal parvalbumin-containing neurons: novel glutamatergic local circuit cells. Hippocampus 14(4):499–509. doi:10.1002/hipo.10195

Henry AM, Hohmann JG (2012) High-resolution gene expression atlases for adult and developing mouse brain and spinal cord. Mamm Genome 23(9–10):539–549. doi:10.1007/s00335-012-9406-2

Hughes DI, Scott DT, Todd AJ, Riddell JS (2003) Lack of evidence for sprouting of Abeta afferents into the superficial laminas of the spinal cord dorsal horn after nerve section. J Neurosci 23(29):9491–9499

Johansson CB, Momma S, Clarke DL, Risling M, Lendahl U, Frisen J (1999) Identification of a neural stem cell in the adult mammalian central nervous system. Cell 96(1):25–34

Kaneko T, Fujiyama F, Hioki H (2002) Immunohistochemical localization of candidates for vesicular glutamate transporters in the rat brain. J Comp Neurol 444(1):39–62

Kasantikul V, Netsky MG, James AE Jr (1979) Relation of age and cerebral ventricle size to central canal in man. Morphological analysis. J Neurosurg 51(1):85–93. doi:10.3171/jns.1979.51.1.0085

Kiehn O (2011) Development and functional organization of spinal locomotor circuits. Curr Opin Neurobiol 21(1):100–109. doi:10.1016/j.conb.2010.09.004

Klausberger T, Somogyi P (2008) Neuronal diversity and temporal dynamics: the unity of hippocampal circuit operations. Science 321(5885):53–57. doi:10.1126/science.1149381

Lagerstrom MC, Rogoz K, Abrahamsen B, Persson E, Reinius B, Nordenankar K, Olund C, Smith C, Mendez JA, Chen ZF, Wood JN, Wallen-Mackenzie A, Kullander K (2010) VGLUT2-dependent sensory neurons in the TRPV1 population regulate pain and itch. Neuron 68(3):529–542. doi:10.1016/j.neuron.2010.09.016

Landry M, Bouali-Benazzouz R, El Mestikawy S, Ravassard P, Nagy F (2004) Expression of vesicular glutamate transporters in rat lumbar spinal cord, with a note on dorsal root ganglia. J Comp Neurol 468(3):380–394. doi:10.1002/cne.10988

Lang B, Liu HL, Liu R, Feng GD, Jiao XY, Ju G (2004) Astrocytes in injured adult rat spinal cord may acquire the potential of neural stem cells. Neuroscience 128(4):775–783. doi:10.1016/j.neuroscience.2004.06.033

Le Maitre E, Barde SS, Palkovits M, Diaz-Heijtz R, Hokfelt TG (2013) Distinct features of neurotransmitter systems in the human brain with focus on the galanin system in locus coeruleus and dorsal raphe. Proc Natl Acad Sci USA 110(6):E536–E545. doi:10.1073/pnas.1221378110

Lein ES, Hawrylycz MJ, Ao N, Ayres M, Bensinger A, Bernard A, Boe AF, Boguski MS, Brockway KS, Byrnes EJ, Chen L, Chen L, Chen TM, Chin MC, Chong J, Crook BE, Czaplinska A, Dang CN, Datta S, Dee NR, Desaki AL, Desta T, Diep E, Dolbeare TA, Donelan MJ, Dong HW, Dougherty JG, Duncan BJ, Ebbert AJ, Eichele G, Estin LK, Faber C, Facer BA, Fields R, Fischer SR, Fliss TP, Frensley C, Gates SN, Glattfelder KJ, Halverson KR, Hart MR, Hohmann JG, Howell MP, Jeung DP, Johnson RA, Karr PT, Kawal R, Kidney JM, Knapik RH, Kuan CL, Lake JH, Laramee AR, Larsen KD, Lau C, Lemon TA, Liang AJ, Liu Y, Luong LT, Michaels J, Morgan JJ, Morgan RJ, Mortrud MT, Mosqueda NF, Ng LL, Ng R, Orta GJ, Overly CC, Pak TH, Parry SE, Pathak SD, Pearson OC, Puchalski RB, Riley ZL, Rockett HR, Rowland SA, Royall JJ, Ruiz MJ, Sarno NR, Schaffnit K, Shapovalova NV, Sivisay T, Slaughterbeck CR, Smith SC, Smith KA, Smith BI, Sodt AJ, Stewart NN, Stumpf KR, Sunkin SM, Sutram M, Tam A, Teemer CD, Thaller C, Thompson CL, Varnam LR, Visel A, Whitlock RM, Wohnoutka PE, Wolkey CK, Wong VY, Wood M, Yaylaoglu MB, Young RC, Youngstrom BL, Yuan XF, Zhang B, Zwingman TA, Jones AR (2007) Genome-wide atlas of gene expression in the adult mouse brain. Nature 445(7124):168–176. doi:10.1038/nature05453

Li JL, Fujiyama F, Kaneko T, Mizuno N (2003) Expression of vesicular glutamate transporters, VGluT1 and VGluT2, in axon terminals of nociceptive primary afferent fibers in the superficial layers of the medullary and spinal dorsal horns of the rat. J Comp Neurol 457(3):236–249. doi:10.1002/cne.10556

Li CL, Li KC, Wu D, Chen Y, Luo H, Zhao JR, Wang SS, Sun MM, Lu YJ, Zhong YQ, Hu XY, Hou R, Zhou BB, Bao L, Xiao HS, Zhang X (2015) Somatosensory neuron types identified by high-coverage single-cell RNA-sequencing and functional heterogeneity. Cell Res. doi:10.1038/cr.2015.149

Liu Y, Abdel Samad O, Zhang L, Duan B, Tong Q, Lopes C, Ji RR, Lowell BB, Ma Q (2010) VGLUT2-dependent glutamate release from nociceptors is required to sense pain and suppress itch. Neuron 68(3):543–556. doi:10.1016/j.neuron.2010.09.008

Ljungdahl A, Hokfelt T, Nilsson G (1978) Distribution of substance P-like immunoreactivity in the central nervous system of the rat—I. Cell bodies and nerve terminals. Neuroscience 3(10): 861–943

Malet M, Vieytes CA, Lundgren KH, Seal RP, Tomasella E, Seroogy KB, Hokfelt T, Gebhart GF, Brumovsky PR (2013) Transcript expression of vesicular glutamate transporters in lumbar dorsal root ganglia and the spinal cord of mice—effects of peripheral axotomy or hindpaw inflammation. Neuroscience 248C:95–111. doi:10.1016/j.neuroscience.2013.05.044

Malmberg AB, Chen C, Tonegawa S, Basbaum AI (1997) Preserved acute pain and reduced neuropathic pain in mice lacking PKCgamma. Science 278(5336):279–283

Milhorat TH, Kotzen RM, Anzil AP (1994) Stenosis of central canal of spinal cord in man: incidence and pathological findings in 232 autopsy cases. J Neurosurg 80(4):716–722. doi:10.3171/jns.1994.80.4.0716

Moechars D, Weston MC, Leo S, Callaerts-Vegh Z, Goris I, Daneels G, Buist A, Cik M, van der Spek P, Kass S, Meert T, D'Hooge R, Rosenmund C, Hampson RM (2006) Vesicular glutamate transporter VGLUT2 expression levels control quantal size and neuropathic pain. J Neurosci 26(46):12055–12066. doi:10.1523/JNEUROSCI.2556-06.2006

Molander C, Xu Q, Grant G (1984) The cytoarchitectonic organization of the spinal cord in the rat. I. The lower thoracic and lumbosacral cord. J Comp Neurol 230(1):133–141. doi:10.1002/cne.902300112

Mori M, Kose A, Tsujino T, Tanaka C (1990) Immunocytochemical localization of protein kinase C subspecies in the rat spinal cord: light and electron microscopic study. J Comp Neurol 299(2):167–177. doi:10.1002/cne.902990204

Navone F, Jahn R, Di Gioia G, Stukenbrok H, Greengard P, De Camilli P (1986) Protein p38: an integral membrane protein specific for small vesicles of neurons and neuroendocrine cells. J Cell Biol 103(6 Pt 1):2511–2527

Oliveira AL, Hydling F, Olsson E, Shi T, Edwards RH, Fujiyama F, Kaneko T, Hokfelt T, Cullheim S, Meister B (2003) Cellular localization of three vesicular glutamate transporter mRNAs and proteins in rat spinal cord and dorsal root ganglia. Synapse 50(2):117–129. doi:10.1002/syn.10249

Polgar E, Fowler JH, McGill MM, Todd AJ (1999) The types of neuron which contain protein kinase C gamma in rat spinal cord. Brain Res 833(1):71–80

Polgar E, Durrieux C, Hughes DI, Todd AJ (2013) A quantitative study of inhibitory interneurons in laminae I-III of the mouse spinal dorsal horn. PLoS One 8(10):e78309. doi:10.1371/journal.pone.0078309

Rehm H, Wiedenmann B, Betz H (1986) Molecular characterization of synaptophysin, a major calcium-binding protein of the synaptic vesicle membrane. EMBO J 5(3):535–541

Ren K, Ruda MA (1994) A comparative study of the calcium-binding proteins calbindin-D28K, calretinin, calmodulin and parvalbumin in the rat spinal cord. Brain Res Brain Res Rev 19(2):163–179

Sabelstrom H, Stenudd M, Reu P, Dias DO, Elfineh M, Zdunek S, Damberg P, Goritz C, Frisen J (2013) Resident neural stem cells restrict tissue damage and neuronal loss after spinal cord injury in mice. Science 342(6158):637–640. doi:10.1126/science.1242576

Sardella TC, Polgar E, Garzillo F, Furuta T, Kaneko T, Watanabe M, Todd AJ (2011) Dynorphin is expressed primarily by GABAergic neurons that contain galanin in the rat dorsal horn. Mol Pain 7:76. doi:10.1186/1744-8069-7-76

Sase S, Sase A, Sialana FJ Jr, Groger M, Bennett KL, Stork O, Lubec G, Li L (2015) Individual phases of contextual fear conditioning differentially modulate dorsal and ventral hippocampal GluA1-3, GluN1-containing receptor complexes and subunits. Hippocampus. doi:10.1002/hipo.22470

Scherrer G, Low SA, Wang X, Zhang J, Yamanaka H, Urban R, Solorzano C, Harper B, Hnasko TS, Edwards RH, Basbaum AI (2010) VGLUT2 expression in primary afferent neurons is essential for normal acute pain and injury-induced heat hypersensitivity. Proc Natl Acad Sci USA 107(51):22296–22301. doi:10.1073/pnas.1013413108

Schwaller B (2010) Cytosolic $Ca^{2+}$ buffers. Cold Spring Harb Perspect Biol 2(11):a004051. doi:10.1101/cshperspect.a004051

Shi TJ, Xiang Q, Zhang MD, Tortoriello G, Hammarberg H, Mulder J, Fried K, Wagner L, Josephson A, Uhlen M, Harkany T, Hokfelt T (2012) Secretagogin is expressed in sensory CGRP neurons and in spinal cord of mouse and complements other calcium-binding proteins, with a note on rat and human. Mol Pain 8:80. doi:10.1186/1744-8069-8-80

Shi TJ, Xiang Q, Zhang MD, Barde S, Kai-Larsen Y, Fried K, Josephson A, Gluck L, Deyev SM, Zvyagin AV, Schulz S, Hokfelt T (2014) Somatostatin and its 2A receptor in dorsal root ganglia and dorsal horn of mouse and human: expression, trafficking and possible role in pain. Mol Pain 10(1):12. doi:10.1186/1744-8069-10-12

Stanic D, Brumovsky P, Fetissov S, Shuster S, Herzog H, Hokfelt T (2006) Characterization of neuropeptide Y2 receptor protein expression in the mouse brain. I. Distribution in cell bodies and nerve terminals. J Comp Neurol 499(3):357–390. doi:10.1002/cne.21046

Sugita S, Sudhof TC (2000) Specificity of $Ca^{2+}$-dependent protein interactions mediated by the C2A domains of synaptotagmins. Biochemistry 39(11):2940–2949

Sugita S, Ho A, Sudhof TC (2002) NECABs: a family of neuronal Ca(2+)-binding proteins with an unusual domain structure and a restricted expression pattern. Neuroscience 112(1):51–63

Talpalar AE, Bouvier J, Borgius L, Fortin G, Pierani A, Kiehn O (2013) Dual-mode operation of neuronal networks involved in left-right alternation. Nature 500(7460):85–88. doi:10.1038/nature12286

Todd AJ, Spike RC, Polgar E (1998a) A quantitative study of neurons which express neurokinin-1 or somatostatin sst2a receptor in rat spinal dorsal horn. Neuroscience 85(2):459–473

Todd AJ, Spike RC, Polgar E (1998b) A quantitative study of neurons which express NEUROKININ-1 or somatostatin sst(2a) receptor in rat spinal dorsal horn. Neuroscience 85(2):459–473. doi:10.1016/S0306-4522(97)00669-6

Todd AJ, Hughes DI, Polgar E, Nagy GG, Mackie M, Ottersen OP, Maxwell DJ (2003) The expression of vesicular glutamate transporters VGLUT1 and VGLUT2 in neurochemically defined axonal populations in the rat spinal cord with emphasis on the dorsal horn. Eur J Neurosci 17(1):13–27

Usoskin D, Furlan A, Islam S, Abdo H, Lonnerberg P, Lou D, Hjerling-Leffler J, Haeggstrom J, Kharchenko O, Kharchenko PV, Linnarsson S, Ernfors P (2015) Unbiased classification of

sensory neuron types by large-scale single-cell RNA sequencing. Nat Neurosci 18(1):145–153. doi:10.1038/nn.3881

Wiedenmann B, Franke WW (1985) Identification and localization of synaptophysin, an integral membrane glycoprotein of Mr 38,000 characteristic of presynaptic vesicles. Cell 41(3):1017–1028

Wu H, Li D, Shan Y, Wan B, Hexige S, Guo J, Wu C, Yu L (2007) EFCBP1/NECAB1, a brain-specifically expressed gene with highest abundance in temporal lobe, encodes a protein containing EF-hand and antibiotic biosynthesis monooxygenase domains. DNA Seq 18(1):73–79. doi:10.1080/10425170500511271

Yasui K, Hashizume Y, Yoshida M, Kameyama T, Sobue G (1999) Age-related morphologic changes of the central canal of the human spinal cord. Acta Neuropathol 97(3):253–259

Zhang MD, Tortoriello G, Hsueh B, Tomer R, Ye L, Mitsios N, Borgius L, Grant G, Kiehn O, Watanabe M, Uhlen M, Mulder J, Deisseroth K, Harkany T, Hokfelt TG (2014) Neuronal calcium-binding proteins 1/2 localize to dorsal root ganglia and excitatory spinal neurons and are regulated by nerve injury. Proc Natl Acad Sci USA 111(12):E1149–E1158. doi:10.1073/pnas.1402318111

Zimmermann B, Girard F, Meszar Z, Celio MR (2013) Expression of the calcium binding proteins Necab-1,-2 and -3 in the adult mouse hippocampus and dentate gyrus. Brain Res 1528:1–7. doi:10.1016/j.brainres.2013.06.004